Master Thesis

Towards the Bottom-Up Synthesis of Low-Energy 3D Allotropes of Carbon

Supervisor at TU Wien:
Univ. Prof. Dr. Dominik Eder

Supervisor at UC Berkeley:
Prof. Dr. Felix R. Fischer

Christoph Bartmann

August 2023

Table of Content

Figures

Tables

Schemes

Abstract

Carbon stands unparalleled in its versatility, arguably making it the most multifaceted element in the universe. Its inherent ability to adopt various hybridization states paves the way for a plethora of structures, materials, and molecules, each with its unique set of properties. Carbon allotropes epitomize this diversity, being compounds composed solely of carbon atoms. While graphite and diamond, the two naturally occurring forms of elemental carbon, are members of this category, the past 35 years have witnessed a renaissance in our understanding and application of carbon-based materials. This period has been marked by groundbreaking strides in materials science, chemistry, and physics, largely propelled by the discovery and exploration of novel carbon allotropes: the 0D buckyballs, 1D carbon nanotubes, and 2D single and multilayer graphene.

Despite tremendous interest in carbonous materials, there has not been any disruption in the category of 3D allotropes. This work represents a starting point in closing the gap of carbon networks, targeting the synthesis of theoretical 3D carbon allotropes specifically 6.8^2 D and 6.8^2 P polybenzene. These nano-porous carbon structures, with their unique electronic attributes and ability to encapsulate various compounds, hold promise for applications in hydrogen storage, spintronics, and battery technology. A novel bottom-up synthesis approach was introduced, leveraging a monomer characterized by 8-membered rings and employing aldol trimerization to form the 6-membered rings.

While the ambitious goal of realizing either polybenzene modification remained elusive, this research successfully established two distinct and scalable synthetic routes, each leading to potential monomers. The study also delved deep into the roles of both Lewis and *Brønsted* acids in polymerization reactions, highlighting the crucial influence of reaction temperatures and solvents on outcomes.

Characterization of the synthesized samples via FT-IR spectroscopy revealed notable differences from the monomer, with reduced carbonyl and alkyl vibrations. Diffraction studies mostly identified the samples as amorphous, but a few exhibited hints of structures with long-range order. Interestingly, reactions involving specific acids, such as CSA, PPTS, and $NbCl_5$, indicated the potential formation of a consistent supramolecular structure. While the journey toward a novel 3D carbon allotrope is still underway, the advancements made in this research signify a promising direction in this challenging domain.

Deutsche Kurzfassung

Kohlenstoff steht in seiner Vielseitigkeit unübertroffen da und ist damit wohl das facettenreichste Element im Universum. Seine inhärente Fähigkeit, verschiedene Hybridisierungszustände anzunehmen, ebnet den Weg für eine Vielzahl von Strukturen, Materialien und Molekülen, jeweils mit einem einzigartigen Eigenschaftsprofil. Kohlenstoffallotrope verkörpern diese Vielfalt, da sie ausschließlich aus Kohlenstoffatomen bestehen. Während Graphit und Diamant, die beiden natürlich vorkommenden Formen des elementaren Kohlenstoffs, Mitglieder dieser Kategorie sind, hat die vergangenen 35 Jahre eine Renaissance in unserem Verständnis und der Anwendung von kohlenstoffbasierten Materialien erlebt. Diese Periode war geprägt von bahnbrechenden Fortschritten in den Materialwissenschaften, der Chemie und der Physik, vor allem durch die Entdeckung und Erforschung neuer Kohlenstoffallotrope: der 0D-Buckybälle, 1D-Kohlenstoffnanoröhren und 2D-Einzel- und Mehrschichtgraphen.

Trotz enormen Interesses an kohlenstoffhaltigen Materialien gab es bisher keine Durchbrüche in der Kategorie der 3D-Allotrope. Diese Arbeit stellt einen Ausgangspunkt dar, um die Lücke in den Kohlenstoffnetzwerken zu schließen und zielt auf die Synthese der theoretischen 3D-Kohlenstoffallotrope, speziell 6.82 D und 6.82 P Polybenzol, ab. Diese nanoporösen Kohlenstoffstrukturen, mit ihren einzigartigen elektronischen Eigenschaften und der Fähigkeit, verschiedene Verbindungen einzuschließen, versprechen Anwendungen in der Wasserstoffspeicherung, der Spintronik und der Batterietechnologie. Ein neuartiger Bottom-up-Syntheseansatz wurde eingeführt, der einen Monomer mit 8-gliedrigen Ringen nutzt und Aldol-Trimerisierung zur Bildung der 6-gliedrigen Ringe einsetzt.

Während das ehrgeizige Ziel der Realisierung einer der Polybenzol-Modifikationen nicht erreicht wurde, hat diese Forschung erfolgreich zwei unterschiedliche und skalierbare synthetische Routen etabliert, die jeweils zu potenziellen Monomeren führen. Die Studie untersuchte auch intensiv die Rollen sowohl von Lewis- als auch von Brønsted-Säuren in Polymerisationsreaktionen und betonte den entscheidenden Einfluss von Reaktionstemperaturen und Lösungsmitteln auf die Ergebnisse.

Die Charakterisierung der synthetisierten Proben mittels FT-IR-Spektroskopie zeigte bemerkenswerte Unterschiede zum Monomer, mit reduzierten Carbonyl- und Alkyl-Schwingungen. Beugungsstudien identifizierten die meisten Proben als amorph, einige zeigten jedoch Anzeichen von Strukturen mit langreichweitiger Ordnung. Interessanterweise deuteten Reaktionen mit spezifischen Säuren, wie CSA, PPTS und NbCl5, auf die potenzielle Bildung einer konsistenten supramolekularen Struktur hin. Obwohl der Weg zu einem neuartigen 3D-Kohlenstoffallotrop noch lang ist, signalisieren die Fortschritte in dieser Forschung eine vielversprechende Richtung in diesem anspruchsvollen Bereich.

Acknowledgments

Firstly, I wish to convey my heartfelt gratitude to Felix. His willingness to respond to my unsolicited email was the beginning of a transformative journey. My tenure in his research group was profoundly enriching, broadening my perspectives on science. I am deeply appreciative of the trust and autonomy you granted me from the outset, fostering an environment where I could thrive.

My sincere thanks also go to my co-supervisor, Prof. Dominik Eder, for his unwavering support at TU Wien. His patience and timely assistance, especially amidst pressing deadlines, were pivotal throughout this endeavor.

I owe a special debt of gratitude to Dr. Carolin Dusold, who partnered with me on this project. Her invaluable guidance and insights were instrumental in achieving the results presented in this thesis. I am also thankful for our enlightening discussions, your empowering leadership style, and the cherished moments shared during our lunch breaks and outside the lab. Additionally, this work would not have come to fruition without the essential chemical supplies generously provided by the Yaghi and Hartwig groups.

A warm acknowledgment to Dr. Sai-Ho Pun, not only for his relentless synthetic advice but also for becoming a cherished friend, adding layers of joy to my experience at Berkely inside and outside of the lab. I also want to express my gratitude to Ethan for the memorable times during our late-night dinners and basketball games. To the entire Fischer research team—Kaitlyn, Christina, Michael, Donnie, Aidan, Adam and Boyu—your welcoming nature from day one made me feel like an integral part of the family. The camaraderie shared with you all was truly a highlight.

The hands-on work for this thesis was undertaken at the University of California, Berkeley. This venture was made feasible by the generous financial backing of the Austrian Marshall Plan Foundation and a scholarship from TU Wien, for which my gratitude knows no bounds.

In closing, my path to this academic milestone has been illuminated by the contributions of numerous remarkable individuals. A special salute to Max, Tobi, and Laurin for their steadfast support and the joy they brought to my university experience; I simply cannot envision this journey without you. Natalia, words fall short in expressing the depth of gratitude I feel for your immense support. You always gave me the energy to keep going. To my parents and siblings, your unwavering support have been my foundation without which I couldn't have achieved any of this. For those not mentioned by name, please know that your contributions have not gone unnoticed or unappreciated.

.

Abbreviations

AcOH	Acetic Acid
BET	Brunauer, Emmett, and Teller
COF	Covalent Organic Framework
CSA	(7,7-dimethyl-2-oxobicyclo[2.2.1]heptan-1-yl)methanesulfonic acid
d	Doublet
DBU	2,3,4,6,7,8,9,10-Octahydropyrimido[1,2-a]azepine
DCM	Dichloromethane
dd	Doublet of Doublet
ddd	Doublet of Doublet of Doublet
dddt	Doublet of Doublet of Doublet of Triplet
DEA	Diethylamine
DMSO	Dimethylsulfoxide
DDQ	2,3-dichloro-5,6-dicyano-1,4-benzoquinone
equ.	Equivalent
EtOAc	Ethylacetate
HRMS	High-Resolution Mass Spectroscopy
IBX	1-hydroxy-1-oxo-1λ^5-benzo[d][1,2]iodaoxol-3(1H)-one
LDA	Lithium N-(propane-2-yl)propan-2-aminide
m	Multiplet
MeOH	Methanol
MSA	Methansulfonic Acid
NBS	1-Bromopyrrolidine-2,5-dione
NMR	Nuclear Magnetic Resonance Spectroscopy
oDCB	Ortho-Dichlorobenzene
PPTS	Pyridium p-Toluenesulfonate
prop. Acid	Propionic Acid
PTSAxH2O	p-Toluenesulfonic Acid Monohydrate
pXRD	Powder X-RAY Diffraction
s	Singlet
t	Triplet
TEM	Transmission Electron Microscopy
TFA	Trifluoroacetic Acid
THF	Tetrahydrofuran

1 Introduction

Carbon, positioned as the 6th element in the periodic table, serves as the foundation for life on Earth. It ranks as the 4th most abundant element in the universe and stands 15th in terms of prevalence within the Earth's crust.[1] Carbon has the unique ability to bond to almost all other elements as well as to itself with three different hybridization states (sp^3, sp^2, sp). This bonding versatility is evident in the fact that carbon is estimated to be present in over 95% of all identified chemical compounds.[2] The vast array of structures among these compounds spans from simple molecules and synthetic organic materials to intricate biomolecules comprising more than 100,000 uniquely positioned carbon atoms. This work focuses on a class of compounds referred to as carbon allotropes, which are exclusively made up of carbon atoms packed into tightly bound crystalline networks.

1.1 Carbon Allotropes

Carbon's remarkable versatility means that the potential number of structures composed solely of carbon is vast, almost beyond comprehension. However, until 1985, conventional scientific wisdom recognized only two allotropes of carbon: the familiar substances of diamond and graphite. When Kroto et *al.*[3] reported their discovery of C_{60}, a fullerene, the situation changed drastically. Since then, various new allotropes of carbon have been proposed and many of them realized.[4–11] The subsequent subsections provide a concise overview of the most notable examples, categorizing them based on their dimensionality.

1.1.1 OD Allotropes

An example of 0D (zero-dimensional) carbon allotropes is the previously mentioned class of fullerenes, with C_{60} (shown in Figure 1) being the smallest stable and most well-known member. This carbon structure was predicted as early as 1970 by Osawa, but his paper, written in Japanese, garnered little attention due to language barriers and the absence of computational chemistry at that time.[12] It consists of a spherical network of sixty structurally equivalent sp^2-hybridized carbon atoms in the shape of a football (or soccer ball) composed of 12 pentagons and 20 hexagons. The first synthesis and characterization was done by Kroto et *al.*[3] in 1985 and sparked the beginning of a new era in carbon research. The ability to produce macroscopic quantities of high-quality fullerenes with relative ease, as first described by Krätschmer and Huffmann,[13] was key to this success.

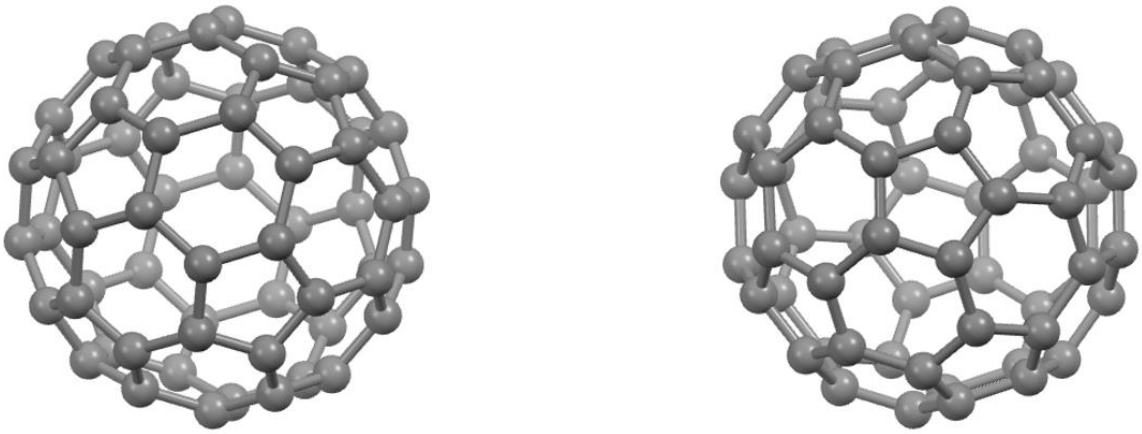

Figure 1: 3D structure model of C_{60}, a 0D carbon allotrope

Several stable fullerenes have been isolated and characterized, including C_{70}, C_{76}, C_{82}, and C_{84}.[3,14] At their core, fullerenes are hollow, closed cages composed of sp^2-hybridized carbon atoms. These atoms are organized into 12 pentagons and a variable number of hexagons, which can be determined based on the total count of carbon atoms. Specifically, a fullerene with 20 + 2n carbon atoms will contain n hexagons. The number of pentagons, dictated by the closed nature of the fullerene structure, remains constant at 12 for those with perfect structures.[15]

The distinct 0D architecture of fullerenes positions them as crucial foundational units for crafting supramolecular assemblies and micro/nano functional materials. These materials find applications in diverse areas, such as optoelectronic devices, catalysis, and biomedicine.[16–18] In particular, C_{60} has a triply degenerate low-lying lowest unoccupied molecular orbital (LUMO), rendering an excellent electron-accepting ability for holding up to six electrons and facilitating the formation of donor-acceptor dyads.[18] This efficient electron transfer capability is arguably the most captivating characteristic of fullerenes, enhancing their desirability in organic photovoltaics (OPVs) and perovskite solar cells (PSCs).[19] Additionally, fullerenes can be viewed as electron-deficient polyalkenes, making them chemically reactive.[7,20] This reactivity facilitates fullerene derivatization, broadening their functional range.

1.1.2 1D Allotropes

Carbon nanotubes (CNTs) stand out as the most notable example of 1D carbon allotropes. The narrative of their discovery remains a topic of debate.[21] As early as 1952, Radushkevich and Lukianovich showcased images of carbon tubes with a 50 nm diameter in the Russian Journal of Physical Chemistry.[22] However, it was only in 1991 that Iijima presented HRTEM images of multi-walled carbon nanotubes (MWCNTs), capturing the scientific community's attention.[9] Two years later the first report of single walled carbon nanotubes was published.[23]

Carbon nanotubes are essentially hollow cylindrical structures formed from sheets of sp^2 hybridized carbon. Conceptually, their structure resembles a rolled-up sheet of a planar hexagonal lattice of carbon atoms, known as graphene (as illustrated in Figure 2) They can be considered as single molecules, regarding their small size (- nm in diameter and m length) or a quasi-one dimensional crystal with translational periodicity along the tube axis. The way the sheet is rolled into a cylinder can vary infinitely, leading to tubes with different diameters and microscopic structures. This variation is determined by the chiral angle, which describes the hexagon's helical orientation around the tube's axis. While certain properties of CNTs can be understood using a macroscopic model of a uniform cylinder, others are intrinsically tied to the tube's microscopic structure. Notably, this includes the electronic band structure, which determines whether the tube is metallic or semiconducting in nature.[24]

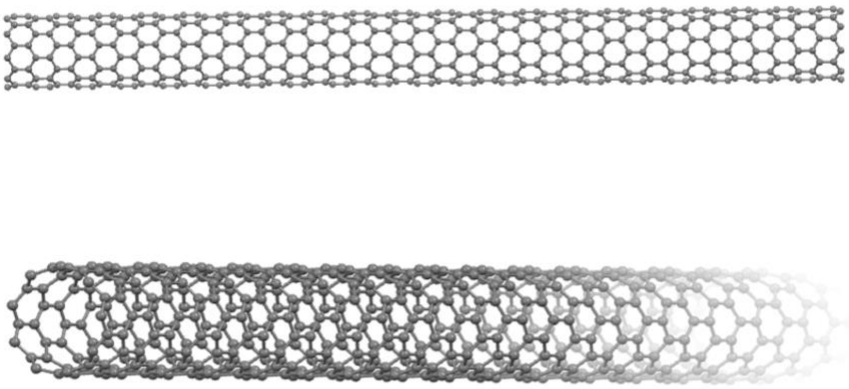

Figure 2: 3D Structure of an open-shelled (9,0) single-walled CNT

CNTs have exhibited remarkable properties both theoretically and experimentally. They boast an impressively high elastic modulus, and strengths that are 10 to 100 times that of the most robust steel, yet at a fraction of the weight. Additionally, CNTs demonstrate exceptional thermal and electrical attributes: they remain thermally stable up to 2800 ˚C in a vacuum, have an electrical conductivity approximating 10^3 S cm^{-1}, and thermal conductivity of about 1900 W m^{-1} K^{-1}, which is about twice as high as diamond.[25] Given these attributes, CNTs hold immense promise across various scientific and technological domains. Potential applications for CNTs span from corrosion protection,[26,27] reinforced materials in natural fiber composites,[28] electromagnetic interference shielding,[29,30] batteries,[31] solar cells,[32] chemical sensors,[25] hydrogen storage,[33] and field-emission materiales.[34]

1.1.3 2D Allotropes

Graphene stands out as the most distinguished example of 2D carbon allotropes. Defined as a flat monolayer of sp^2 carbon atoms densely arranged in a two-dimensional honeycomb lattice, graphene serves as the foundational unit for graphitic materials across all dimensions. It can be

transformed into 0D fullerenes, rolled to form 1D nanotubes, or layered to produce 3D graphite. While the theoretical exploration of graphene (often termed "2D graphite") spans seven decades,[35,36] it wasn't until 2004 that Novoselov and Geim[10] were able to fabricate single layers of graphene through mechanically exfoliating graphite. Not only were they able to characterize the novel allotrope, which was previously thought to be unstable, but were also able to fabricate a field effect transistor. The measured conductivity was incredibly high, turning graphene based research into one of the hottest topics in science.[37]

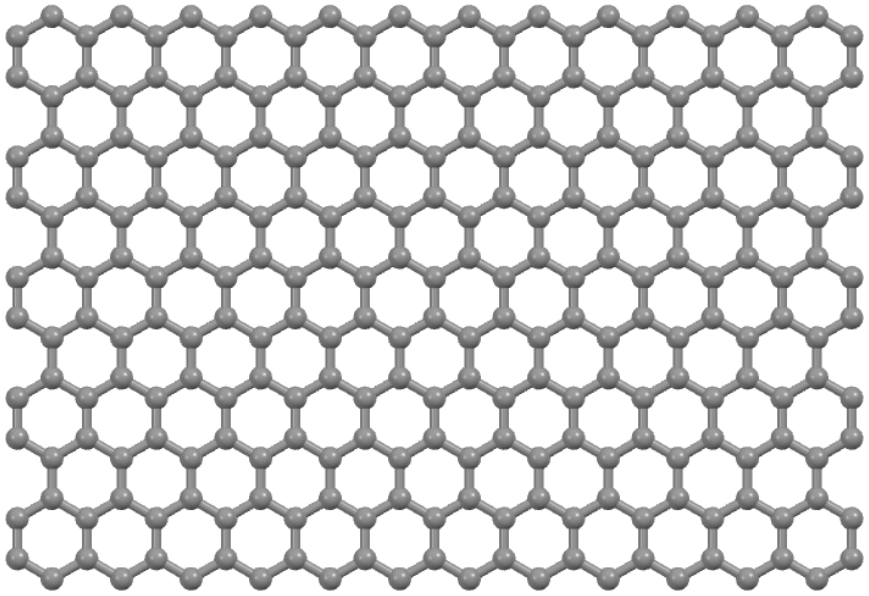

Figure 3: 3D Structure of single layer graphene from the top

Experimental evaluations of graphene's properties have often surpassed those of any other known material, with some even approaching theoretical maxima: room-temperature electron mobility of 2.5 3 105 cm^2 V^{-1} s^{-1}; [38] Young's modulus of 1 TPa and intrinsic strength of 130 GPa;[39] very high thermal conductivity of above 3,000 W mK^{-1};[40] optical transparency of approximately 97.7%;[41] ability to sustain extremely high densities of electric current (a million times higher than copper).[42] Another property of graphene is that it can be readily chemically functionalized.[43] Consequently, graphene has garnered immense attention in the research community, finding applications in diverse areas such as sensing, field-effect transistors (FETs), energy conversion and storage, catalysis, and more.[44–47]

1.1.4 3D Allotropes

Besides the two natural three dimensional allotropes of carbon, diamond and graphite, the family of 3D SCA (Structurally Complex Allotropes) is still largely limited to theoretically predicted modifications.

The primary distinction between diamond and graphite lies in their carbon bonding: diamond employs sp^3 hybridization, while graphite utilizes sp^2 hybridization. Consequently, diamond exhibits a three-dimensional crystal lattice, whereas graphite is composed of carbon layers. Within each of these layers, covalent and metallic bonds are present. These layers, known as graphene layers,[48] are stacked in an AB sequence and held together by weak van der Waals interactions, a result of delocalized pi-orbitals (as depicted in Figure 4)

Graphite's nature is anisotropic. It conducts electricity and heat efficiently within its layers, courtesy of the in-plane metallic bonding. In contrast, its conductivity is poor perpendicular to the layers, attributed to the weak van der Waals forces between them. This electrical conductivity positions graphite as a prime candidate for electrochemical electrodes. The inherent anisotropy also allows the carbon layers to slide over one another with ease, making graphite an effective lubricant and the primary material for pencils.[48]

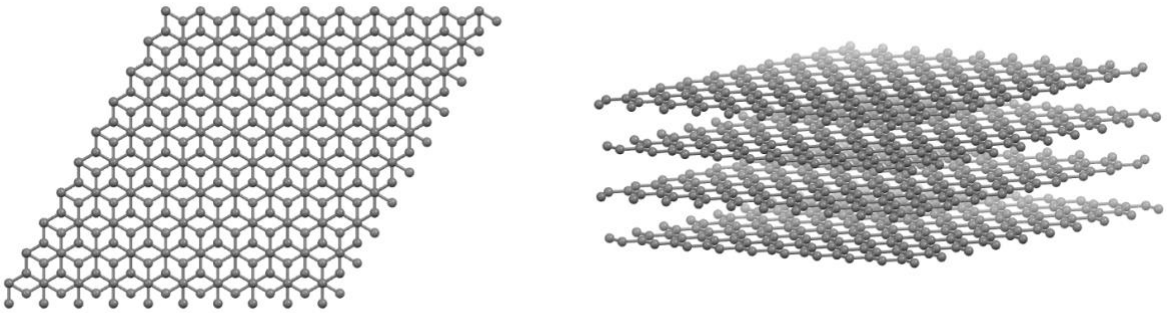

Figure 4: 3D structure of graphite from the top (left) and side (right)

Diamond, on the other hand, is structured with carbon atoms interconnected through tetrahedral sp^3 hybrid orbitals, forming a face-centered cubic (fcc) crystal system (illustrated in Figure 5). The robust covalent bonds within diamond give rise to its unique properties. Notably, it's the hardest known material and simultaneously boasts the lowest thermal expansion coefficient. Other notable characteristics include its chemical inertness, high wear resistance, exceptional thermal conductivity, electrical insulation, and broad optical transparency, spanning from ultraviolet (UV) to far infrared (IR) wavelengths.[49] Predominantly, diamonds are employed in applications where their inherent, unchanging properties are utilized, such as their hardness in cutting tools and abrasives, or their thermal conductivity in thermal management, rather than in roles where they undergo dynamic or reactive changes.[50]

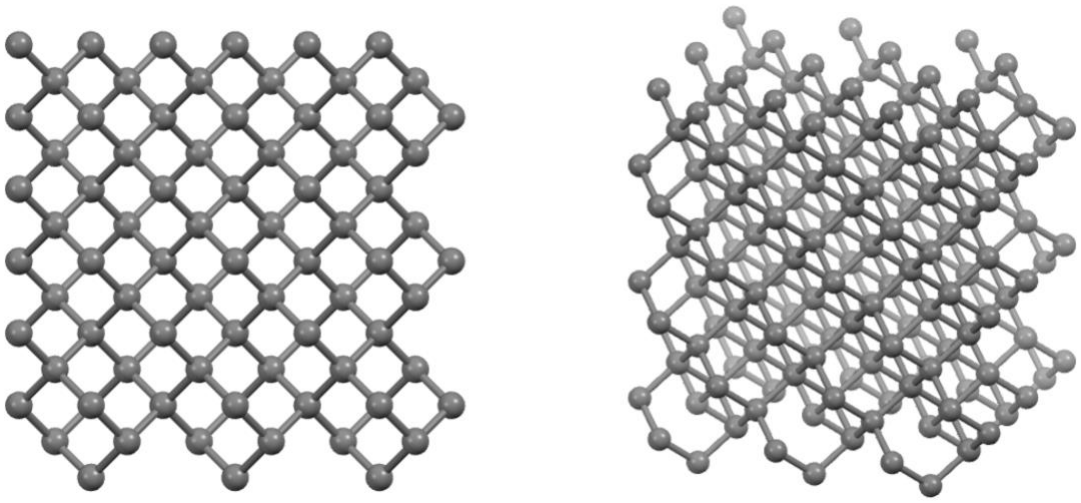

Figure 5: 3D structure of diamond from the top (left) and perspective (right)

1.2 Polybenzene

The discovery of new carbon allotropes over the past forty years as well as their recognition via the Nobel Price sparked a rally to theoretically predict and discover other novel forms of carbon.[4,6,8,11,51,52] A notable yet elusive category in this domain is the family known as polybenzenes. First proposed by O'Keeffe, Adams, and Sankey in 1992[6,53] these structures are part of the so far undisrupted subsection of 3D carbon allotropes. There have been several theoretical discussions on this group of compounds and this section aims to summarize the most important points for the two target compounds of this work.

A defining trait of polybenzenes is the sp^2 hybridization of each carbon atom, resulting in three equivalent bonds. The most rudimentary tiling of a 3-periodic minimal surface, characterized by a singular vertex type (in this context, an sp^2 hybridized carbon atom), is epitomized by the structures labeled as 6.8^2 D and 6.8^2 P, as illustrated in Figure 6. While additional tilings are conceivable, they are deemed less probable due to the necessity to integrate highly strained 3- and 4-membered rings. The minimal surfaces, designated P for primitive and D for diamond, manifest as a maze-like system of pores, echoing the topologies of the primitive cubic (pcu) and diamond (dia) structures. The dual nets of this tiling are realized through a 6-membered ring and two 8-membered rings converging at each vertex. This configuration is thus termed 6.8.8 or 6.8^2, as per Schläfli symbols.

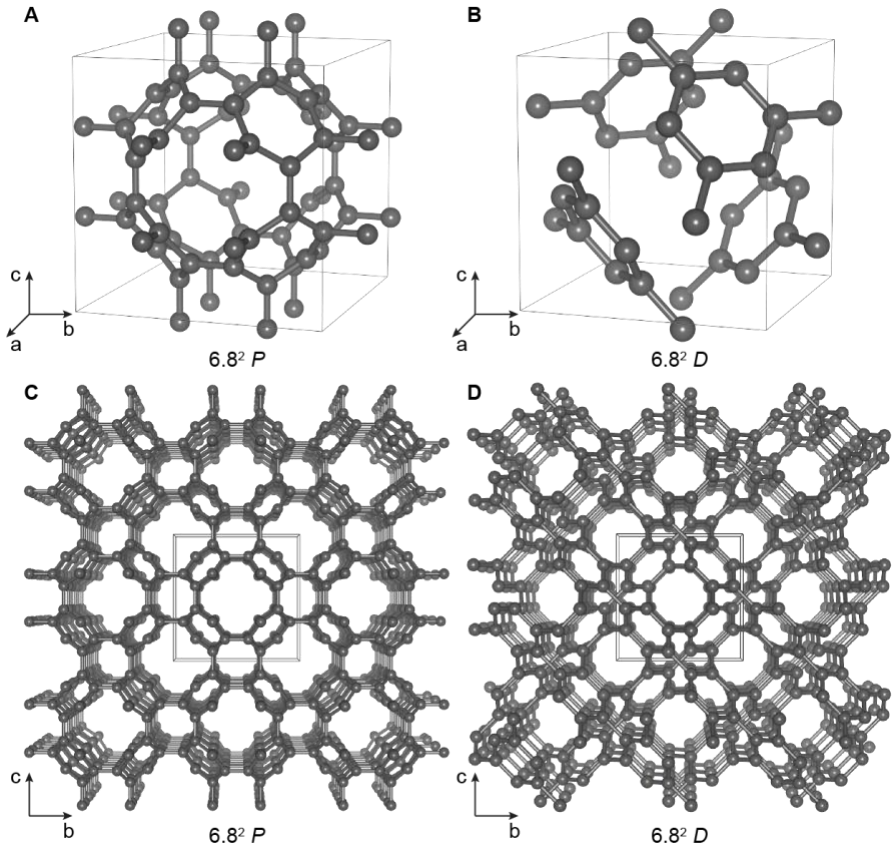

Figure 6: DFTB optimized structures of the unit cell of (A) 6.82 P and (B) 6.82 D. A 3×3×3 model for the crystallographic packing of (C) 6.82 P and (D) 6.82 D in a cubic lattice.

The extended structure of 6.8^2 *P* polybenzene can be seen as a cubic tiling of truncated C_{60} fullerenes joined to six identical structures along with the faces of a cube (Figure 6C). The resulting linkages give rise to eight-membered rings adopting a boat conformation. The C–C bond length in six-membered and eight-membered rings is 1.410 Å and 1.327 Å, respectively, suggesting a network of cyclooctatetraenes fused by six-membered rings along the edges of the single bonds. Despite the obvious angle strain required to adopt the cyclooctatetraene boat conformation, C–C–C = 117.1°, 120.1°, and 120.1°, the overall stability of 6.8^2 *P* polybenzene (ΔE = 0.488 eV per C-atom) is comparable to that of C_{60} fullerene (ΔE = 0.438 eV per C-atom; all energies are referenced to the carbon atom in unstrained graphene).

The structure of the second polymorph, the 6.8^2 *D* polybenzene tiling (Figure 6B), is much more reminiscent of the parent's name of this class of 3D carbon allotropes. The unit cell may be thought of as four aromatic benzene rings arranged on the faces of a tetrahedron. In the extended crystal, the benzene rings link up into orthogonally stacked layers of poly-para-phenylene chains featuring a dihedral angle of 70.5° around the C–C single bond (1.417 Å) linking two neighboring benzene rings (Figure 6D). The C–C bond length within the planar six-membered rings (1.395 Å) is reminiscent of that observed in benzene (1.39 Å) while all C–C–C bond angles adapt to the ideal trigonal planar geometry of 120.0°. We thus may consider the structure of 6.8^2 *D* polybenzene to be comprised of planar aromatic benzene rings linked into a 3D network

through C–C single bonds. It is therefore not surprising that 6.8^2 *D* (ΔE = 0.208 eV per C-atom) is much more stable than the angle strained 6.8^2 *P* polymorph.

Both 6.8^2 structures feature large cavities within the crystal lattice suitable for the intercalation of small molecules or ions. In 6.8^2 D the approximate volume enclosed by the tetrahedral arrangement of benzene rings in the unit cell is ~8.4 Å^3, more than large enough to accommodate Li^+, Na^+, Mg^{2+}, or Ca^{2+} ions. The pores in 6.8^2 *P* polybenzene are significantly larger (~23.6 Å^3) and would accommodate even bigger cations and anions like K^+, Rb^+, Sr^{2+}, F^-, Cl^-, Br^- or even small diatomic molecules like CO, N_2, NO, or O_2.

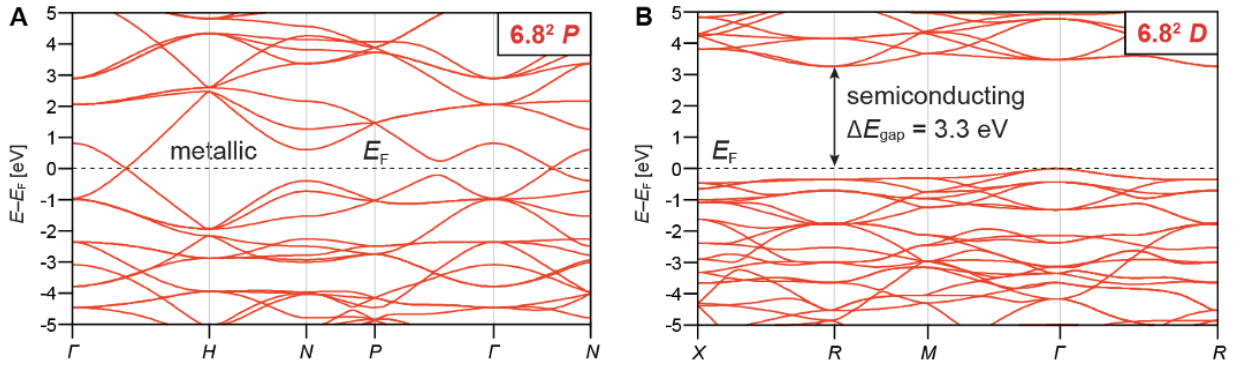

Figure 7: Electronic band structure of DFTB optimized structures of (A) 6.8^2 *P* and (B) 6.8^2 *D*. 6.8^2 *P* is a metal while the 6.8^2 *D* polymorph is an indirect semiconductor with a bandgap of ΔE_{gap} = 3.3 eV.

The subtle structural differences in the bonding between carbon atoms in 6.8^2 *P*, a 3D network of cyclooctatetraenes, and 6.8^2 *D*, a 3D network of aromatic benzene rings, are also reflected in their characteristic electronic structures. The DFTB calculated band structure of 6.8^2 *P* polybenzene is depicted in Figure 7A and shows two frontier bands crossing the Fermi level (E_F). The 6.8^2 *P* polymorph is therefore a metal with a significant band dispersion, high charge carrier mobilities, and a low mass of charge carriers. In contrast, the 6.8^2 *D* polymorph is an indirect bandgap semiconductor (Figure 7B). The bandgap of 6.8^2 *D* polybenzene (ΔE_{gap} = 3.3 eV) is significantly smaller than the experimental HOMO–LUMO gap of aromatic C_6H_6 benzene ($\Delta E_{exp.}$ = 10.3 eV)[54] suggesting a strong interaction of the π-system of the C_6 benzene fragments in the crystal lattice despite the large dihedral angle (70.5°) adopted by the planes of adjacent aromatic rings.

1.3 Reticular Chemistry

While many periodic structures come to light through serendipity, the deliberate design and assembly of such materials at the molecular level remains a coveted objective in scientific research. In the past twenty years, reticular chemistry has emerged as a potent tool for the prediction and design of a myriad of periodically extended structures.[55–57] This domain revolves around the assembly of distinct molecular building blocks, interconnected by robust bonds, into crystalline extended frameworks. Such an approach has paved the way for the synthesis of a wide array of metal-organic frameworks (MOFs) and covalent organic frameworks (COFs). What sets

these structures apart is their customizable nature; their pore shape, size, and functionality can be meticulously tailored to suit specific applications.[58] Since the present work aims to bottom-up synthesize a 3D crystalline porous network of covalently bound carbon atoms, our discussion will center exclusively on covalent organic frameworks.

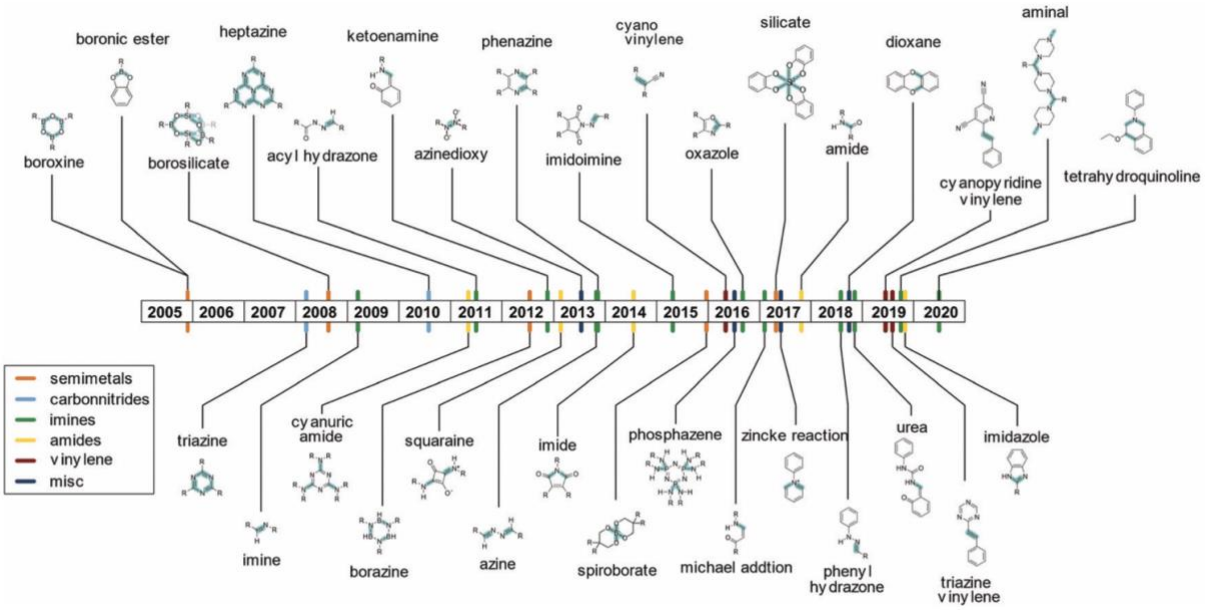

Figure 8: Various linkages for COF synthesis, categorized by their reversible covalent bond formation, are presented alongside their respective debut dates in scholarly publications. The bond created during COF linkage is highlighted in cyan.[59]

Since the pioneering work by Yaghi et *al.* in 2005,[60] which introduced the use of boronic ester building blocks to craft the inaugural COF, a plethora of reactions has been investigated and documented for COF synthesis. (Illustrated in Figure 8) Initially, the emphasis was predominantly on borate-based COFs. However, the landscape shifted rapidly with the advent of imine linkages in 2009,[61] which now hold a commanding presence in the COF domain. Over time, a diverse array of reactions has been developed, with a selection showcased in Figure 8. Subsequent sections will delve into general considerations essential for crafting a sturdy, crystalline covalent organic network. A simple overview of the strategies at one's disposal is depicted in Figure 9.

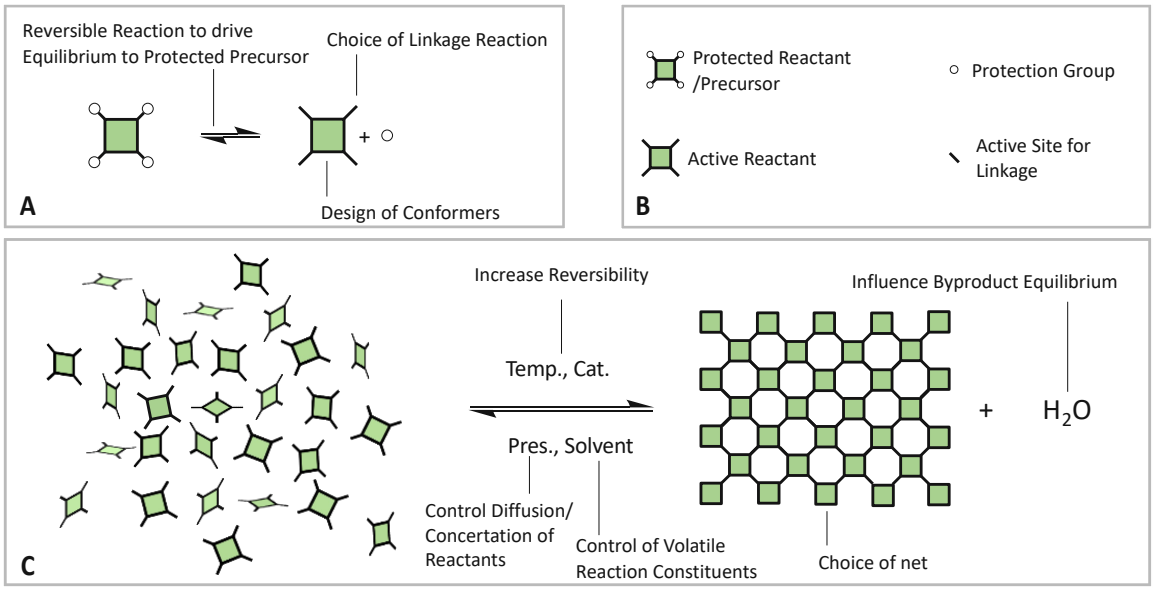

Figure 9: Concise summary of methods for generating crystalline organic networks, featuring essential techniques. (A) Reversible reaction unveils active linking sites by deprotecting the reactant. (B) Legend for interpretation. (C) General COF crystallization reaction involving multiple monomers to form a crystalline structure. Modified from Haase et *al.*[59]

1.3.1 Reversible Bond Formation

The quintessential strategy for crafting crystalline organic frameworks leverages the principles of dynamic covalent chemistry (as depicted in Figure 10), which means it relies on reactions that allow for reversible covalent bond formation during the synthesis. The reversible bond enables the building blocks to arrange in the thermodynamic minimum configuration.

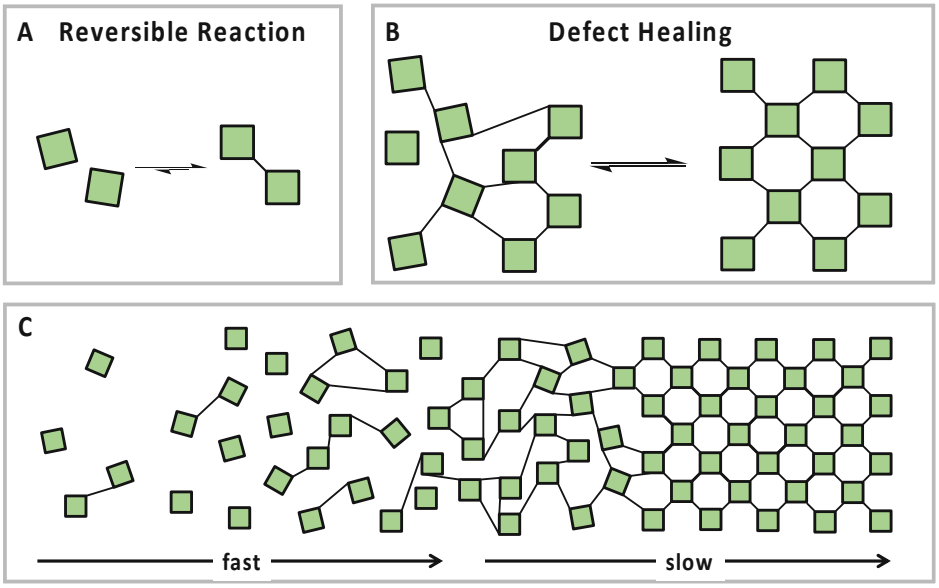

Figure 10: Essential factors for achieving crystalline networks: (A) Reversible reactions as a key ingredient. (B) Defect healing through sufficient energy and time, as suggested by imine condensation. (C) Slow crystallization process leading to imine-based COF structures, starting from an amorphous gel. Figure adapted from Hasse et *al.*[59]

If the structure is not crystalline or contains defects, dangling bonds, off-equilibrium structures are produced, which are energetically less favorable than the corresponding ordered structure. The reversible nature of the bond formation, however, offers a corrective or "self-healing" mechanism. This process capitalizes on the energy advantage to enhance the crystallinity of the structure.[62]

The pathway to achieving a crystalline network can vary significantly based on the underlying reaction mechanism. For instance, in the synthesis of boronic ester COFs, the initial stages involve the formation of sheet-like oligomers and crystallites under reversible conditions in a solution. These entities then undergo precipitation via stacking and aggregation. Subsequent crystallization processes are then constrained by kinetic factors.[63] Conversely, the synthesis of imine COFs adheres to a distinct mechanism. Here, an amorphous polymer forms rapidly, which is then gradually transformed into a crystalline material over time.[64,65]

1.3.2 Role of water

Achieving a crystalline material necessitates a comprehensive understanding and control of all facets of the reaction. For reactions characterized by condensation mechanisms, the equilibrium is profoundly influenced by the water content. As demonstrated by systematic studies from Dichtel et *al.*,[64] in imine condensations, incrementally increasing the water content promotes the reverse reaction in COFs, thereby enhancing COF crystallization. When an acetic acid catalyst was introduced without water, the swift forward reaction resulted in the formation of amorphous imine polymers. However, the introduction of an adequate amount of water alongside the catalyst yielded an ordered material.[64] This underscores the notion that the water produced intrinsically through a condensation reaction (in this context, the imine reaction) might not be ample to facilitate the reverse reaction, and consequently, crystallization.
For amide COFs, the regulation of water vapor pressure has been identified as pivotal in achieving crystalline structures. It's been documented that amide COFs can be synthesized from an amorphous prepolymer. This is achieved by subjecting the prepolymer to a reaction within a sealed tube, containing a meticulously calibrated amount of water, resulting in COFs exhibiting commendable crystallinity.[66]

1.3.3 Role of catalyst

The pivotal role of catalysts in determining the crystallinity of COFs is evident. Catalysts, by virtue of reducing the activation barrier of a reaction, can enhance its reversibility, thereby promoting crystallinity. However, there's a caveat: excessive catalyst can overly accelerate the reaction, leading to the formation of an amorphous structure instead. While acetic acid is a commonly employed catalyst for imine COFs, the exploration hasn't been confined to it. A gamut of alternative catalyst systems has been investigated. For instance, various *Brønsted* acids, such as sulfonic acids, have been effectively utilized, as demonstrated by Banerjee et *al.*[67,68] Furthermore, Lewis acids have also been recognized as viable catalysts, both for the synthesis of boronic ester COFs[63] and imine COFs.[69] Notably, the employment of Lewis acid catalysis in the creation of imine COFs has yielded materials with markedly enhanced crystallinity and augmented porosity when juxtaposed with COFs synthesized using acetic acid catalysis.[69,70]

1.3.4 Enhancing reversibility

The significance of a reaction's reversibility, especially in the context of achieving high crystallinity in COFs, cannot be overstated. Beyond the evident influences of catalysts and reaction by-products like water, there are other innovative strategies that have been employed. Bein et *al.*[71] pioneered a modulator approach to enhance crystallization in the synthesis of boronic ester COFs. This method involves slowing down the nuclei's growth, thereby favoring the reverse reaction. By introducing a monodentate boronic acid alongside the bidentate boronic acid linker, they observed sharper reflections in pXRD, augmented BET surface areas, and larger domain sizes as captured by TEM. The modulator's role is to decelerate the growth of COF crystallites by swiftly binding to their surface, which in turn reversibly hinders the attachment of new linkers.[71]
Banerjee et *al.* [67] work offers another example. They devised a technique that promotes the reverse reaction by converting the amine into a salt of p-toluenesulfonic acid. This acid multitasks as a catalyst, templating agent, inhibitor of the COF-forming reaction, and an agent that encourages the reverse reaction. The initial reaction is slowed down as the protonated amine must first be deprotonated to partake in the imine bond formation within the COF. Moreover, the presence of this potent acid modulates the equilibrium between imine formation and hydrolysis, leaning towards hydrolysis via the protonation of the free amine. This innovative approach not only enhanced the crystallinity of twelve distinct COFs, confirming its broad applicability, but also amplified surface areas by two to threefold compared to traditional solvothermal processes.[67]

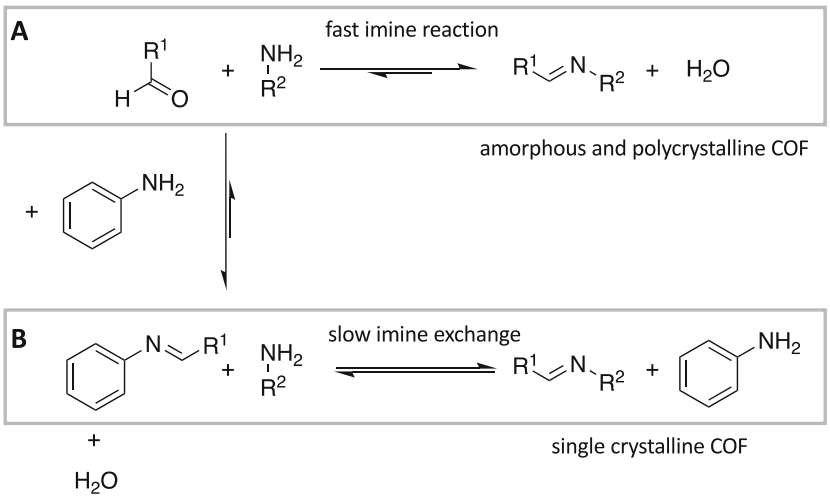

Scheme 1: Imine exchange strategy developed by Wang, Sun, Yaghi, et al.[72] successfully employed for single crystal COF synthesis. (A) Classic imine reaction leading to amorphous or polycrystalline COF networks. (B) Reaction rate is moderated by adding Aniline, which is gradually replaced by another amine reactant, resulting in single crystalline COFs. Scheme adapted from Wang, Sun, Yaghi, et al.[72]

Building on the foundational concept of modulators in COF synthesis, Wang, Sun, Yaghi, et *al.*[72] made a groundbreaking advancement. They successfully grew COF single crystals of a size amenable to analysis by single-crystal X-ray diffraction. By adding a monodentate aniline, they

fine-tuned the reaction equilibrium of the imine formation to such a degree that, for the first time, the X-ray single-crystal structure of 3D imine COFs could be solved. The monofunctional amines in the reaction vie with the linker in producing the imine, slowing the reaction, and amplifying the reverse reaction. To enhance crystallinity using the modulator, various anilines were trialed. Only those matching the reactivity of the linkers led to crystallinity enhancements. Otherwise, the outcome was either diminished crystallinity or the production of amorphous materials.[72] The overarching framework of this innovative approach is outlined in Scheme 1.

1.3.5 Pre-orientation of building blocks

The synthesis of amorphous materials through strong covalent bonds under non-reversible conditions is a straightforward endeavor. Similarly, crystallizing materials using only weak interactions is also relatively simple due to the high reversibility of these interactions. The pre-orientation strategy bifurcates the processes of ordering and the formation of (often irreversible) covalent bonds into sequential steps, enabling the production of COFs that are both highly crystalline and stable.

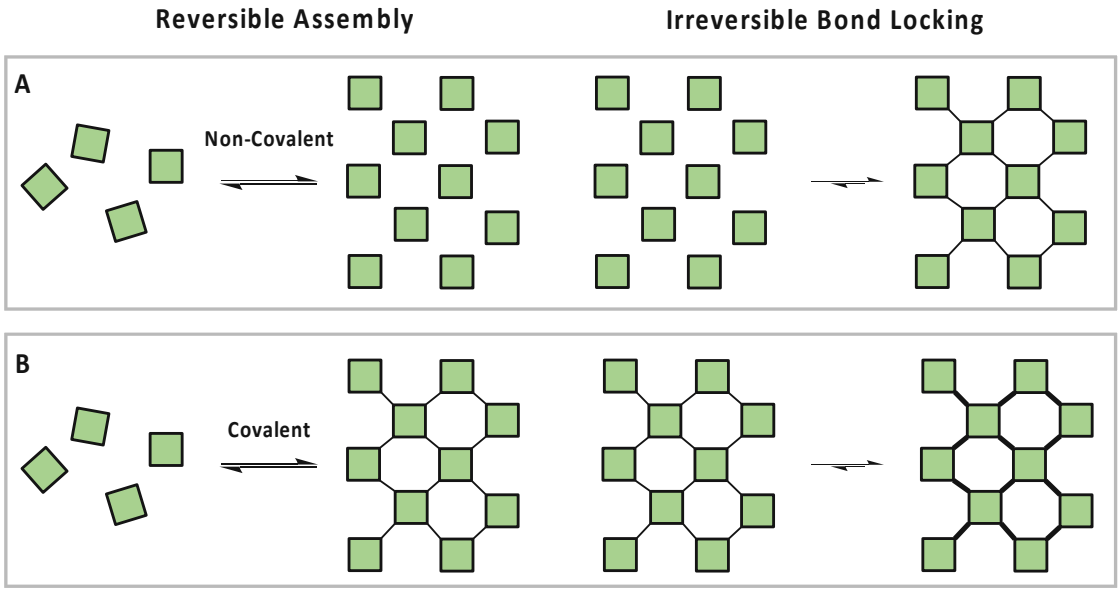

Figure 11: Two-step COF formation via pre-orientation: Initial reversible alignment of building blocks sets the stage for irreversible stabilization of the ordered structure. (A) Non-covalent pre-orientation followed by covalent bond formation. (B) Initial reversible covalent bonding, succeeded by irreversible locking of the labile bond. Figure modified from Hasse et *al.*[59]

During the order-inducing phase, building blocks are systematically oriented and ordered via a highly reversible reaction. The resulting pre-oriented intermediate can exhibit varying degrees of fragility, contingent on the nature of the reaction used to establish the ordered state. This spectrum ranges from non-covalently bonded molecular crystals to weakly covalently bonded solids. Subsequently, in the stability-inducing phase, the building blocks of the pre-ordered assembly are interconnected with robust bonds, often through an irreversible reaction. The choice of reaction and its conditions ensures that the previously achieved order is preserved and solidified.

The concept of pre-orientation has been applied across various material classes, but its traction in the COF domain has been particularly notable, especially with studies underscoring the viability of linkage conversion in COFs.[73] The foundational principle of pre-orientation bears resemblance to classical templating effects, which have been harnessed in the synthesis of mesoporous silica[74,75] and two-dimensional polymers.[76] However, these instances typically exhibit only long-range order, with the materials often being disordered at molecular scales. By modulating the interactions of reactive building blocks at the molecular level, it becomes feasible to induce short-range order, thereby facilitating the synthesis of crystalline materials that might otherwise be challenging to produce. A case in point is zeolites, where this strategy has been employed to create 'unfeasible' zeolites[77] by pre-orienting exfoliated crystalline layers using ionic stacking modulators that dictate the stacking sequence. This pre-arranged assembly is subsequently solidified by irreversibly binding the layers through reactive silanes. This method paves the way for the creation of crystalline zeolites that would be challenging to produce via direct solvothermal methods.[77,78] This exemplifies how pre-orientation can be applied across scales, from mesoscopic to molecular, to yield crystalline structures.

The success of this widespread pre-orientation strategy hinges on four essential prerequisites: The reversible assembly must remain intact under the conditions of the stability-inducing step; The building blocks must be oriented correctly to enable the reaction to proceed; The material's order must withstand any forces generated during or as a result of the transformation; The reagents and catalysts must access the COF linkage and execute the reaction, even in a sterically challenging environment. By satisfying these conditions, the pre-orientation strategy opens up new avenues for the synthesis of complex crystalline materials, expanding the possibilities within the field of COFs and beyond.

1.3.6 Slow supply of building blocks

In the synthesis of COFs based on reversible reactions, the gradual introduction of reactants has been recognized as a critical factor, as first noted in the seminal COF paper by Yaghi et *al.*[3] The diffusion of precursors was carefully controlled by selecting solvents that adjusted the solubility of the linkers. This choice of solvents in COF synthesis is paramount when seeking conditions that yield crystalline COFs, underscoring the potential importance of controlling the feed rate in the formation of all COFs.[114]

Investigations into the mechanism of boronate COF formation have revealed that once precipitation of oligomers and COF sheets takes place, only minimal improvements in crystallinity can be achieved, suggesting that further crystallization is obstructed.[18] This finding implies that a reduced initial reaction rate can help prevent the kinetic trapping of a COF with low crystallinity. Building on these insights, strategies have been devised to slow down the initial reaction speed For example, Dichtel and co-workers[27] demonstrated that protecting amine precursors, such as benzophenone imines, can decelerate the initial reaction speed. In this approach, the amine must first be deprotected before it can participate in the formation of the COF. This delayed reaction process leads to enhanced crystallinity, providing a valuable technique for controlling the structure and properties of COFs.

1.3.7 Designing COFs with a low number of structural degrees of freedom

The number of potential conformers directly influences the degrees of freedom at the local building block level, which in turn affects the growth of oligomers and the eventual formation of the COF. This influence primarily manifests as disorder and flexibility within the COF structure. Therefore, by reducing the degrees of freedom within the building block, one can significantly impact the growth trajectory of a COF and its resulting crystallinity.

The earliest COFs, which were based on boronic ester and boronic acid anhydride linkages, were designed with minimal conformational degrees of freedom. This inherent rigidity made their crystallization more straightforward. In COF reactions that exhibit limited reversibility, having a low number of conformers might be crucial for achieving crystallinity. This is evident in COFs based on irreversible reactions.

Loh et *al.*[79,80] provided a compelling demonstration of this principle. They successfully coupled several flat, rigid aromatic bromo precursors through an uncatalyzed Ullmann coupling at elevated temperatures to produce COFs. In this instance, the inherent rigidity of the building blocks and linkages compensated for the absence of error correction and healing mechanisms typically provided by reversible reactions.

Furthermore, the cyclotrimerization of nitriles to produce COFs is characterized by its low reversibility.[81] As a result, only a handful of crystalline examples have been reported, and all of them rely on building blocks with minimal conformers.[82–84] In contrast, COFs derived from building blocks with a higher number of conformers tend to be amorphous.[85–87]

1.4 Monomer Design

After discussing the structural features of both target polybenzene polymorphs as well as general strategies to achieve crystalline organic frameworks we can utilize this knowledge for the design of a monomer suitable for the reticular synthesis of the target carbon allotropes.

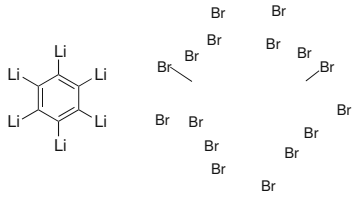

Figure 12: Molecular building blocks for 6.8^2 *D* 6.8^2 *P* polybenzene previously proposed in the literature.

Since the theoretical prediction by O'Keeffe, Adams, and Sankey in 1992 [6,53] polybenzenes have sparked the discussion of several building blocks, which range from hexalithiated benzene to perhalogenated tetrabenzocyclooctatetraene (shown in Figure 12). These formally can be considered viable molecular precursors, which could tile into the structures of both 6.8^2 *D* and 6.8^2 *P* polybenzene. These compounds, however, are extremely unstable and reactive. Therefore, even if they could be achieved synthetically, they violate the strategies to achieve crystalline organic frameworks (Section 1.3) and thus would most likely lead to a network of amorphous carbon.

The underlying challenge in the design of a competent molecular precursor is that the bonds formed during the 3D crystal growth phase are all covalent C–C bonds. These thermodynamically stable bonds tend to form irreversibly and in the absence of any superior catalyst, control would

lead to largely non-crystalline carbon. As discussed in section 1.3, it is of upmost importance to guarantee that any bonds formed are either restricted by predesigned conformations or remain reversible to enable error corrections.

Structurally both 6.8^2 *P* and 6.8^2 *D* are made up of six- and eight-membered rings in a ratio of 2:3. Naturally, it makes sense to incorporate either or both motives already in the design of the monomer precursor. Building up an eight-membered ring during the crystal growth is synthetically much more challenging than the six-membered one. Additionally, taking into account that within the 6.8^2 *D* polymorph the six-membered rings can be considered aromatic. (Section 1.2) The buildup of tris annulated benzene rings via the aldol cyclotrimerization is a well-established reaction. This reaction proceeds through a sequence of three iterative aldol condensations. In the presence of water, each of these intermediate steps is reversible. The final step, the elimination of water from the trimer intermediate to yield the aromatic benzene core represents the driving force. The proposed mechanism is shown in Scheme 2 and is discussed in more detail in Section 1.5.

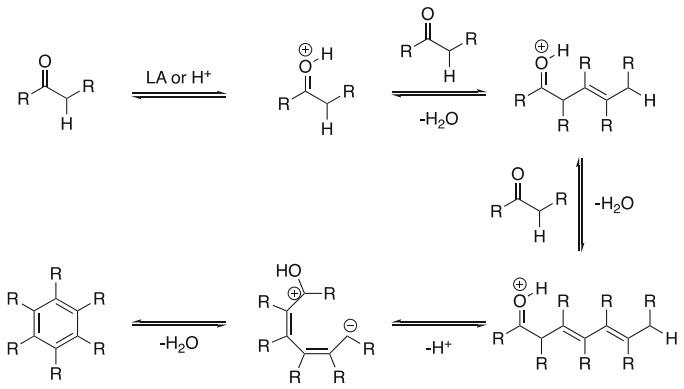

Scheme 2: Mechanism for the cyclotrimerization of aliphatic ketones to give tri- and hexasubstituted benzenes.

Translation of this chemistry into the design of a competent molecular precursor for 6.8^2 *D* and 6.8^2 *P* polybenzene requires the retrosynthetic disconnection of all six-membered benzene rings in the polybenzene structure into aliphatic ketone/enolate equivalents. This approach is diametrically opposed to any previously suggested designs that had relied on the much more challenging formation of the 8-membered rings during the crystal growth. Following this concept, the key molecular building block for both the structure of 6.8^2 *D* and 6.8^2 *P* polybenzene is represented by the cycloocta-1,3,5,7-tetraone (**1**) depicted in Figure 13. With this monomer, a sequence of iterative *Lewis* or *Brønsted* acid catalyzed enolizations followed by self-condensations will drive the reaction towards the extended 3D structures of 6.8^2 *D* and 6.8^2 *P* polybenzene. If the reaction is performed in the presence of trace amounts of water the reversibility of the aldol condensation mechanism will allow for the crucial dynamic error correction during the reticular growth.

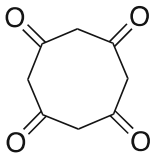

1

cyclooctane-1,3,5,7-tetraone

Figure 13: Proposed molecular building block for 6.8^2 *D* 6.8^2 *P* polybenzene based on reversible dynamic ketone cyclotrimerization mechanism.

Theoretical calculations in the gas phase predict that the 6.8^2 *D* polymorph of polybenzene is 0.23 eV per C-atom more stable than the 6.8^2 *P* polymorph (Section 1.2). It is therefore reasonable to expect that under unbiased reaction conditions the predominant product will be the

semiconducting polymorph 6.8^2 *D*. To access the metallic 6.8^2 *P* polymorph, comparable in stability to C_{60} fullerene, utilizing a templating strategy seems feasible. Adding different metal cations of larger size (e.g. K^+, Rb^+, Sr^{2+}) during the solvothermal synthesis will bias the formation of the lattice featuring the larger internal pores, i.e. the metallic 6.8^2 *P* polymorph. Underlining this hypothesis, is the fact that the pores in 6.8^2 *D* and 6.8^2 *P* are lined by aromatic rings that mimic the characteristic cation-π interaction[88,89] environment encountered in biological receptors and artificial host-guest complexes. Additionally, this approach is reminiscent of the one taken in the synthesis of unfeasible zeolites as described in Section 1.3.5.

1.5 Aldol Trimerization

The aldol trimerization serves as the foundational approach for our bottom-up synthesis of the polybenzene network. Given its significance, a comprehensive understanding of this reaction is paramount. Historically, the aldol trimerization of cyclic ketones has been recognized since the 19th century as a synthetic route to produce tris-annulated benzene rings. This method has been extensively utilized in the synthesis of tri- and hexasubstituted aromatic rings,[90–94] extended polycyclic aromatic hydrocarbons,[95] and even as molecular templates to achieve single chirality in carbon nanotubes[96] Notably, many of these trimers align with the surface structure of C_{60}, positioning them as potential precursors in the chemical synthesis of fullerenes.[95] Scheme 2 illustrates the general assumed mechanism of this reaction. The culminating formation of a benzene ring in the final step likely accounts for the consistently high yields observed in various listed literature examples.

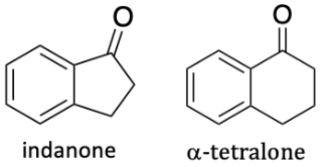

Figure 14: Structural formula of indanone and α-tetralone

The aldol trimerization, despite its historical significance, still presents ambiguities regarding its scope and limitations. This ambiguity largely stems from its unpredictable nature. For instance, while certain ketones readily yield trimeric products with high efficiency, others predominantly lead to acyclic dimers, higher oligomers, or complex mixtures of products. A case in point is the comparison between indanone and α-tetralone as depicted in Figure 14. Under identical reaction conditions, indanone yields truxene with an impressive 98% yield,[97] while the latter doesn't yield any measurable quantities of the tris condensate product.[98]

In light of these inconsistent results from the literature, Amick and Scott proposed several criteria and considerations for a successful aldol trimerization:[99]

- The intermediate formed during the initial condensation should be α,β-unsaturated.
- The dimer must stay in the solution.
- Elevated temperatures are not mandatory.
- The choice of solvent should consider both polarizability and a degree of polarity.
- Both Lewis and *Brønsted* acids are viable catalysts. However, overly potent *Brønsted* acids might favor polymerization over cyclization.

While these guidelines provide a foundational understanding for aldol trimerization, they are not definitive. As the authors themselves acknowledge, a comprehensive methodology for the aldol trimerization of cyclic ketones remains a work in progress. Adding to the complexity is the fact that aldol trimerization has never been documented to occur multiple times on a singular molecule. Consequently, the relevance of these guidelines for the condensation of the proposed monomer **1** remains uncertain. Therefore, the literature conditions are not discussed in further detail. Nonetheless, it underscores the monumental challenge posed by the synthesis of any polybenzene network via aldol trimerization. If the behavior of aldol trimerization in constructing a covalent organic network mirrors that of smaller molecules, it necessitates a comprehensive screening process.

2 Aim of this Thesis

The ultimate goal of this thesis is to close the gap between novel carbon allotropes in the third dimension. While articulating this aim is straightforward, its realization is considerably intricate. Drawing inspiration from landmark achievements in carbon allotropes, such as fullerenes and graphene, this work similarly aims to synthesize the previously theoretically predicted 3D carbon allotrope 6.8^2 *D* and 6.8^2 *P* polybenzene. The strategy revolves around the reticular self-assembly of a specially designed monomer, with the aldol trimerization reaction serving as the pivotal reaction mechanism.

The first step to reaching this goal is the synthesis of cycloocta-1,3,5,7-tetraone (**1**). This compound epitomizes the symmetry of the most rudimentary molecular building block that aligns with the crystal structure of polybenzene. A primary objective is not merely the synthesis of this literature unknown molecule but also the establishment of a scalable synthetic pathway. This scalability is crucial, given the often capricious nature of aldol trimerization, necessitating a thorough screening of conditions during polymerization.

For the actual realization of the novel carbon allotrope, we will harness the reticular self-assembly of the molecular precursors we synthesize. Several strategies exist for the fabrication of crystalline organic frameworks. However, given that our proposed reaction mechanism is uncharted territory for synthesizing such networks, iterative optimization of growth conditions becomes essential. The aim is to identify conditions that permit limited reversibility of the cross-linking reaction, thereby facilitating error correction throughout the crystal growth phase. In the concluding stages, we will probe the potential of solvent and/or cation templating effects to unlock the thermodynamically less favored 6.8^2 *P* polymorph of polybenzene.

3 Results and Discussion

3.1 Synthesis of the Monomer

While the desired precursor remains undocumented in existing literature, two closely related derivatives have been reported: the tetraspirocyclopropanated cyclooctatetraone[100] and the tetraenolether, which emerges from the deprotonation and O-alkylation of cyclooctatetraone[101] Directly adopting the synthesis of these derivatives appears impractical, given that the target compounds were obtained only in minimal quantities. Highlighted in preceding sections, synthesizing any form of polybenzene polymorph is anticipated to be a complex undertaking. Consequently, the ability to scale becomes a paramount feature for any synthetic route directed towards compound **1**.

Despite its seemingly straightforward structure, the synthesis of the target compound is more intricate than initially presumed. This research introduces two distinct synthetic pathways leading to two derivatives of **1**. These derivatives can serve as precursors for the construction of either the 6.8^2 *P* or 6.8^2 *D* polybenzene network. As anticipated, the journey to pinpoint both a functional and scalable synthetic route demanded extensive experimentation and iterative refinement.

3.1.1 Synthetic Pathway A

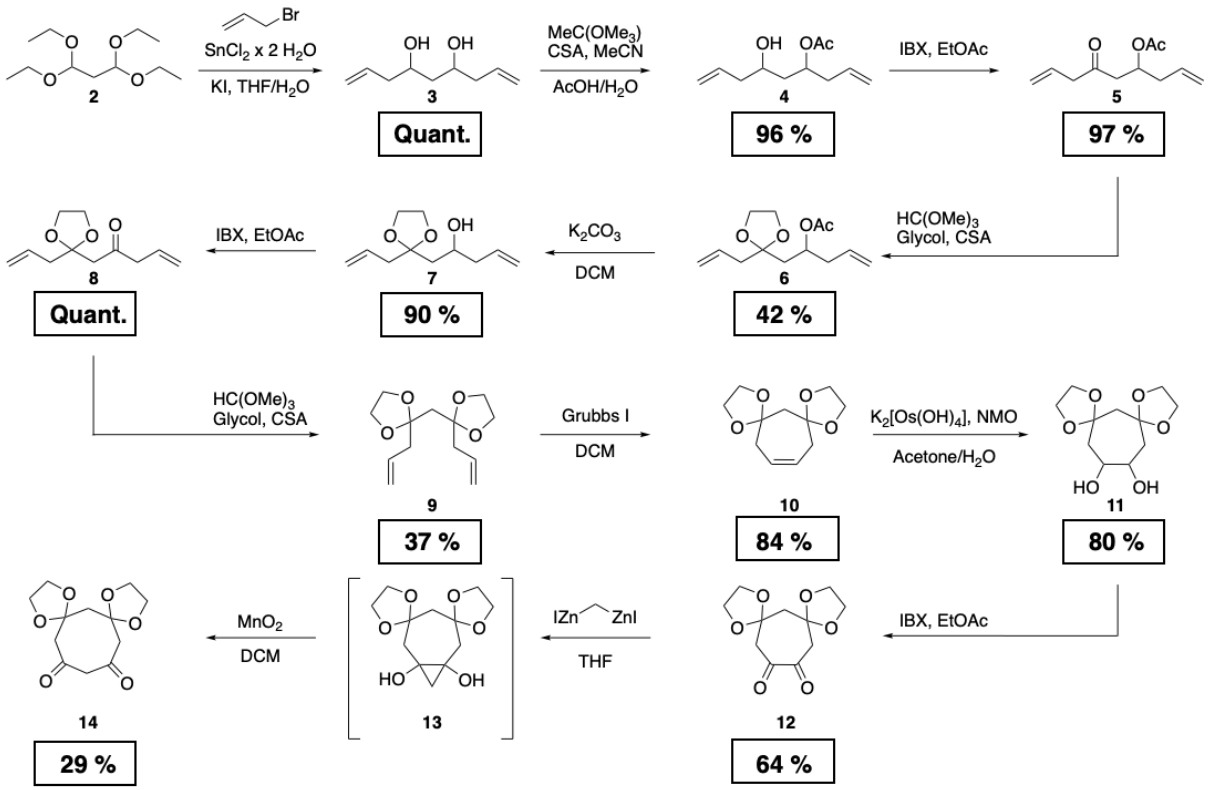

Scheme 3: Synthetic pathway A towards the synthesis of compound 14

The first of the developed synthetic routes are discussed in this section and displayed in Scheme 3. It starts with the treatment of the masked malonaldehyde **2** with a stannane, derived from allyl bromide, which yields an unsaturated diol **3**. This is a literature known reaction[102] and was performed on a big scale without the need for any purification. Therefore, it is a good starting point for any scalable synthesis. The next step is the protection of one of the secondary alcohols (**4**) followed by oxidation of the remaining hydroxyl group to the ketone using IBX yields the nonanone **5** in high quantities. Afterward protection of the carbonyl group as the 1,3-dioxolane ketal **6** was performed. This is now the first reaction where the yield drops below 50% and where purification in the form of column chromatography was necessary.

Extensive optimization experiments were performed, however, the yield could never be improved above the reported 42%. Using classic protection procedures, which utilize refluxing heat and trap water either using mol sieves or a dean stark condenser didn't yield the product at all. Switching the protecting group from ethylene glycol acetal to dimethyl acetal also didn't show any improvement. Essential for successful protection is beside the reaction temperature, the reaction time. When leaving the reaction mixture for 72 hours the yield of the reaction dropped to 11%.

There is no clear explanation as to why this reaction is so low yielding. The protection of a ketone using acetals is a standard procedure in organic chemistry and has been demonstrated to work on an array of different compounds in reliable high yields.[103] Trying to avoid this detour and oxidizing the diol **3** to the diketone and performing the protection of both moieties at the same tie in one reaction did not yield the product **9** at all. Therefore, the stepwise oxidization and respective protections were necessary.

The synthesis continues with the hydrolysis of the acetyl group, yielding the secondary alcohol **7**. A subsequent oxidation using IBX, followed by protection of the resultant ketone (**8**), produces the bis-1,3-dioxolane **9**. Notably, the sole step necessitating purification in this sequence is the protection step, which delivers the product in a moderate yield of up to 37%. A summary of several optimization attempts is presented in Table 1.

Table 1: Examples of optimization attempts to synthesize **9**

Glycol	Orthoformate	Solvent	Conc.	Catalyst	Temp. (˚C)	Yield
1.1 equ	-/mol sieves	Toluene	0.02 mM	PTSA (10%)	110	-
15 equ.	3 equ.	DCM	0.1 mM	CSA (5%)	24	20%
3 equ.	2 equ.	DCM	0.2 mM	$BF_3 \bullet Et_2O$ (5%)	- 78	-
3 equ.	2 equ.	Toluene	0.09 mM	CSA (5%)	110	-
10 equ.	-/mol sieves	Glycol	1 mM	CSA (5%)	24	traces
10 equ.	4 equ.	DCM	0.6 mM	CSA (5%)	24	30%
20 equ.	4 equ.	Glycol	1 mM	CSA (2%)	24	35%
20 equ.	4 equ.	Glycol	1 mM	CSA (5%)	24	37%

Similar to the earlier discussed reaction, elevated temperatures appear to be counterproductive, irrespective of the choice of water-trapping agent. Employing a Lewis acid in lieu of a *Brønsted* acid also does not seem to facilitate product formation. Conversely, augmenting the quantity of the moderate drying agent, trimethyl orthoformate, optimizes the reaction's outcome. Attempts to dilute the reaction mixture or employ alternative solvent systems did not enhance the yield.

The *Grubbs* ring-closing cross metathesis transforms the terminal double bonds, yielding a pivotal intermediate: the protected cycloheptene **10**. To round off the reaction sequence, the double bond in intermediate cycloheptene **10** can be subjected to Upjohn dihydroxylation conditions, producing the syn-diol **11**.[104] Both these reactions are characterized by their simplicity and commendable yields. However, it's worth noting that both stages necessitate column chromatography for purification. Oxidizing the diol with IBX furnishes the diketone **12**. In contrast to prior oxidation steps, this reaction exhibits a marginally reduced yield. This discrepancy might be attributed to the fact that this specific reaction was conducted only once, and thus, the yield may not represent an optimized value. Furthermore, purification via column chromatography was essential, which, while ensuring a high product purity, contributed to a decreased yield.

The Matsubara-type [2+1] cyclopropanation of the diketone, employing bis(iodozincio)methane, facilitated the synthesis of the bicyclic geminal diol **13**.[105,106] Through screening various methods for the preparation of the Simmons-Smith reagent, a dependable technique was established, enabling the synthesis of compound **13** in substantial quantities. A pivotal discovery was that high dilution was instrumental in achieving a high yield for the cyclopropanation.

Compound **13** was used without further purification and finally, oxidative ring expansion using MnO_2 gave the double-protected derivative of the desired molecular building block cycloocta-1,3,5,7-tetraone (**1**) in an overall yield over 2 steps of 29%. Attempts to change the oxidative agent to e.g. IBX, $Pd(OAc)_2$, etc. could not improve the yield.

Attempts to deprotect **14** failed to produce the target compound **1**. This outcome might suggest that compound **14** is excessively reactive to be isolated effectively. However, as elaborated in Section 1.3, employing the protected monomer might be advantageous for achieving a highly crystalline COF. The gradual release of monomers (in this context, active sites) is a recognized strategy to bolster crystallinity in reticular chemistry. Consequently, the monomer was directly employed in its protected form for all polymerization experiments, as detailed in Section 3.2.

3.1.2 Synthetic Pathway B

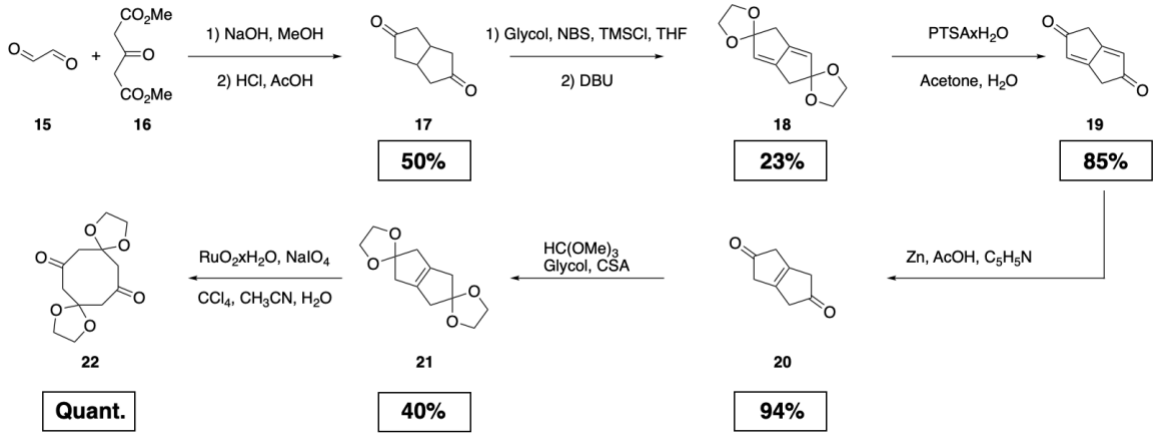

Scheme 4: Synthetic pathway B towards the synthesis of compound **22**

The second synthetic route is designed to construct the synthetically challenging 8-membered ring from the outset, circumventing the reliance on the somewhat low-yielding ring expansion employed in synthetic pathway A. The entire route is illustrated in Scheme 4. It starts with a literature known Weiss-Cook reaction, first reported in 1968[107] and used successfully several times since then.[108–110] Utilizing the methodology compound **17** was synthesized in moderate yield based on previous reported literature.[108] Recrystallization served as an effective purification method, delivering the product in its pure form.

The transformation of ketones to the more versatile enone functionality stands as a pivotal maneuver in organic synthesis. The induction of an alkene adjacent to a ketone is well-established in literature and can be broadly bifurcated into two primary categories: two-step methods that progress via an α-functionalized intermediate and one-step methods that directly transition from ketones to enones in a singular operation.[111,112] The two-step strategies encompass the halogenation of an alpha carbon followed by elimination under the influence of a base and elevated temperatures. A frequently adopted two-step approach is the Saegusa-Ito oxidation, which demands the synthesis of a transient enoxysilane in its initial phase.[113] The subsequent oxidation, mediated by palladium, has been executed with catalytic loadings. However, stoichiometric amounts of the precious metal are often indispensable to circumvent the emergence of the proto-desilylation byproduct.[114] An alternative strategy involves the substitution of the alpha carbon using sulfur or selenium reagents, which, post an oxidative phase, can be readily eliminated.[115] Direct one-step conversions encompass the methodology pioneered by Nicolaou[116], who showcased that a stoichiometric hypervalent iodine oxidant, 2-iodoxybenzoic acid (IBX), can facilitate the α,β-dehydrogenation of ketones and aldehydes. The direct transformations involve the deployment of nonselective oxidants, such as 2,3-dichloro-5,6-dicyano-1,4-benzoquinone (DDQ).[117]

The direct synthesis of compound **19**, using established protocols from the literature, either failed to produce the desired product or resulted in only trace amounts. A summary of the explored reaction conditions can be found in Table 2. This outcome is somewhat unexpected,

especially considering that the formation of a singular enone moiety on compound **17**, for both its protected and unprotected derivatives, has been documented.[108,118] A plausible explanation for the failure of some of these reactions lies in the potential formation of the double bond. If it forms not on the intended bicyclic rings but on the same one, a cyclopentadienone derivative emerges. Compounds of this class are notoriously reactive and unstable, which would lead them to undergo further reactions, preventing the formation of the desired product.[119]

Table 2: Examples of reaction conditions used to directly synthesize **19**

Reaction Conditions	Yield
Br_2, AcOH	-
1) Br_2, AcOH 2) DBU	-
1) LDA, TMSCl 2) $Pd(OAc)_2$, O_2	2 %
IBX, DMSO	-
1) NaH, PhSOOMe 2) K_2CO_3, Toluene	6 %
DDQ, PTSAxH_2O	-
1) PhSeSePh, $K_2S_2O_8$ 2) H_2O_2, C_5H_5N	-
1) LDA, $PhSeCl_3$ 2) K_2CO_3	-

Given these findings, a more circuitous route was deemed the most viable approach to synthesize **19**. By concurrently protecting, halogenating, and then eliminating, the protected enone **18** was obtained in significantly superior yields compared to any direct synthesis attempts, as detailed in Table 2.

Efforts to enhance the yield of this reaction were undertaken by segmenting the simultaneous process into three distinct reactions, as depicted in Scheme 5. Predictably, the protection of both ketones proceeded efficiently, yielding compound **23**. The subsequent bromination step produced the dihalogenated compound **24**, albeit with a modest yield. Intriguingly, the elimination process adhered to an E2-type elimination mechanism. In the presence of a non-polar solvent, no elimination was discernible. However, the introduction of a polar solvent, such as DMSO, facilitated the formation of compound **18**. The yield remained relatively consistent across different bases.
When juxtaposing the yields from this tripartite synthesis of intermediate **18** with the one-pot approach, the merits of the latter become evident. The concurrent reaction, as illustrated in Scheme 4 , not only boasts a superior yield for compound **18** but also streamlines the process by reducing the number of steps and requisite purification stages.

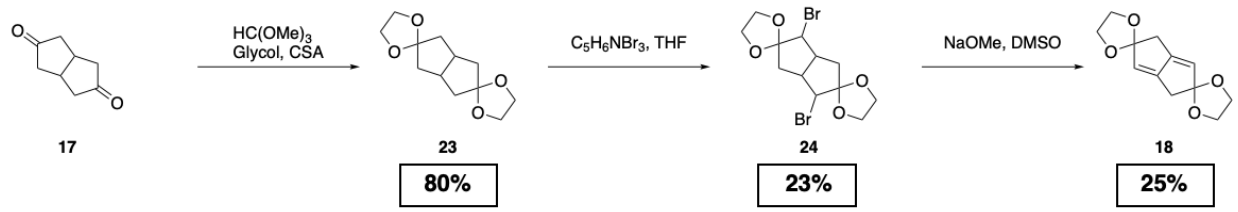

Scheme 5: Stepwise synthesis of intermediate **18**

The removal of both ketal protecting groups to yield compound **19** was accomplished using PTSA as a catalyst, and as anticipated, this step proceeded with high efficiency. The subsequent reduction of the double bond represents a pivotal juncture in this synthetic route. While this reaction might not be classified as a routine synthetic procedure, it has been documented on two distinct occasions: once in a publication[120] over four decades ago, specifically for the same compound, and more recently in a 2008 patent,[121] which focused on a derivative of compound **19**. The reaction unfolded in alignment with the literature descriptions, facilitating the synthesis of compound **20** without necessitating further purification.

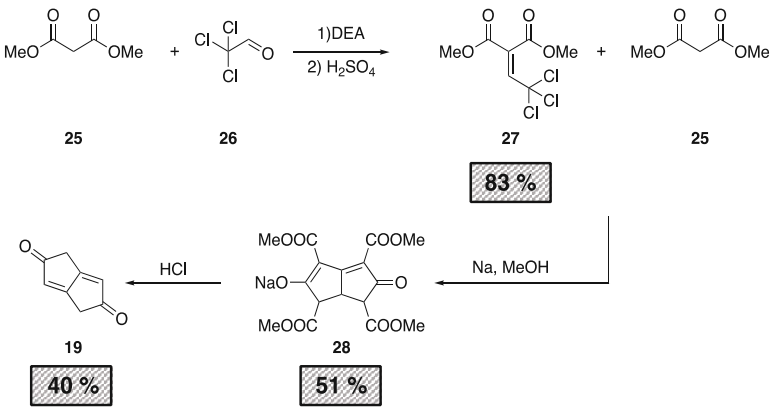

Scheme 6: Alternative synthetic route to intermediate 19, as documented in the literature. Yields are as reported in publications by Docken[120] and Vossen et al.[122] and have not been independently reproduced in this work.

Integrating the methodologies of Docken[120] and Vossen et *al.*[122] offers an alternative synthetic pathway towards the pivotal intermediate **19**. (as shown in Scheme 6) However, this route presents several drawbacks when compared to the approach detailed herein. Firstly, the reproducibility of the synthesis from the literature is challenging to ascertain, given its origin in 1910. The landscape of synthetic procedures and analytical techniques has undergone significant evolution since that time. Moreover, the yield reported in this older literature is marginally inferior to that achieved through our developed route Another concern is the starting material: Chloral (**26**), derived from chloral hydrate, is classified as a Schedule IV controlled substance, which can introduce regulatory and procurement challenges. Furthermore, Vossen's synthesis mandates the use of stoichiometric quantities of sodium. This requirement could introduce substantial safety hazards, especially when scaling up the reaction to the requisite gram quantities.

Following the reduction, the carbonyl groups are concurrently protected to yield compound **21**. When juxtaposed with the protection yields in synthetic route A, the outcome of this step is notably commendable. One potential rationale for this discrepancy could be the differing scales on which these reactions were executed. However, when benchmarked against other ketal protections documented in the literature, the yield appears modest. This diminished yield might be attributed to the inherent instability of compound **20**. Docken previously highlighted the compound's instability in protic solvents, noting its propensity to undergo color changes over time. Given this observation, it's conceivable that immediate protection under aprotic conditions, as delineated by Noyori et *al.*[123] , might bolster this yield, thereby enhancing the viability of the entire synthetic pathway.

The synthesis culminates with an oxidative cleavage, introducing the two requisite carbonyl functional groups to produce compound **22**. Given the well-established nature of this reaction, its successful outcome was anticipated[124–126] However, endeavors to execute the same transformation on the unprotected intermediate **20** failed to yield the target compound **1**. This suggests that the proposed monomer might either be excessively reactive, leading to decomposition, or it might spontaneously undergo aldol condensations even under relatively mild acidic conditions. However, as already mentioned the use of a protected monomer might be beneficial in the following COF synthesis. The nuances distinguishing both synthetic routes and the inherent properties of the monomers will be elaborated upon in the subsequent section.

3.1.3 Comparison of the Synthetic Routes

Synthetic pathways A and B both give access to two different derivates of cycloocta-1,3,5,7-tetraone (**1**), which are potential monomers for the synthesis of both 6.8^2 *D* and 6.8^2 *P* modifications of polybenzene.

Synthetic route A is a 12-step process, necessitating six column chromatography purifications. Three reactions emerge as clear bottlenecks in this route: the dual protections of the ketone functional group, the cyclopropanation reaction, and the subsequent oxidative cleavage. Extensive optimization efforts have been invested in this route, with the yields depicted in Scheme 3 representing the final, optimized values. A significant advantage of this route is its scalability; all reactions, barring the final two, were executed on a gram scale, underscoring its potential for larger-scale applications.

In contrast, synthetic pathway B is more concise, comprising six steps. It demands four column chromatography purifications and a single recrystallization. Two reactions stand out as potential bottlenecks: the synthesis of the enone intermediate and the protection of the ketone functional groups. Not all reactions in this pathway were executed on a large scale, and given the insights from route A, the final protection step might encounter challenges during scale-up.

From a practical standpoint, synthetic route B appears more favorable. It boasts fewer reaction steps and requires less purification. However, the overall yields of both routes leave room for improvement. Route A's cumulative yield stands at 1.4%, while route B achieves a slightly better 3.7%. It's crucial to note that the yields from route A are based on predominantly gram-scale

reactions, whereas route B's are not. This discrepancy could potentially equalize the yields of the two routes when scaled up.

Both monomers, **14** and **22**, indeed hold promise as precursors for the synthesis of either polymorph of polybenzene. However, their distinct symmetries offer unique considerations. Specifically, monomer **14** possesses a mirror plane bisecting the molecule's center, while **22** is characterized by an inversion center. This difference in symmetry is evident in the respective ^{1}H-NMR spectra of the two molecules. The spectrum of **14** presents three distinct signals, whereas that of **22** displays a singular signal. This heightened symmetry in **22** might confer advantages during reticular synthesis. It's important to note, however, that this symmetry difference pertains only to the protecting groups and not the core monomer itself.

Another crucial factor to consider is the aldol trimerization mechanism, which fundamentally relies on the formation of an enolate. For monomer **14**, generating an enolate at at least one active site is a reasonable expectation. This could result in a slower rate of active site availability, potentially leading to a crystalline network. On the other hand, the formation of an enolate in compound **22** is impeded by the location of its protective group. The necessity to remove this protective group before any condensation occurs could be viewed as an additional factor that even further slows down the reaction.

However, any definitive preference for one derivative over the other must be substantiated by experimental data. As of now, making a conclusive choice between the two based on their inherent properties remains speculative.

3.2 Polymerizations

Any attempt to synthesize either polybenzene target was done using compound **14**. This was done purely based on the time of completion of the respective route and not on any symmetry or reactivity considerations. As underscored in section 1.5, the behavior of the aldol trimerization reaction can be quite erratic. Adding to the complexity, the literature lacks reports of this reaction being applied multiple times on a single molecule, as is the intent here. Given these challenges, a rigorous screening process was initiated. A broad range of conditions, encompassing both Lewis and *Brønsted* acids, various solvents, and a spectrum of temperatures, were meticulously examined. In cases where a precipitate emerged post work-up, the resultant powder was subjected to analytical scrutiny using infrared (IR) spectroscopy and powder X-RAY diffraction (pXRD). The subsequent subsections will detail the findings from these explorations.

3.2.1 Precipitation

The initial indication of a successful polymerization was the emergence of a precipitate. Table 3 enumerates all the Lewis acids that were screened. The rationale behind their selection was grounded in prior literature, where certain Lewis acids had been demonstrated to effectively catalyze the aldol trimerization. Notable examples include $TiCl_4$,[94] $SiCl_4$,[90,127,128] $ZrCl_4$,[129] and PTSA/$SnCl_4$. The remaining Lewis acids were chosen to encompass a diverse array of transition metals and varying acid strengths. The outcomes of these reactions are catalogued in Table 3.

To elucidate the terminology employed: "precipitation" refers to the emergence of a solid-like substance during the reaction within the closed system. As detailed in Section 5, any resultant compound underwent a washing process using a spectrum of solvents spanning a wide polarity range. If a solid remained post these steps, it was termed "residue". Precipitation was a frequent observation across most trials. However, reactions conducted at room temperature did not result in any solid formation, hinting at a potential necessity for elevated temperatures. This observation inherently restricts the screening process, given the low boiling points of several organic solvents.

Interestingly, the trials employing Titanium- and Tin-halides completely dissolved upon workup, leaving no residue behind. This observation underscores that precipitation does not necessarily equate to the formation of a supramolecular structure. It's plausible that low molecular weight oligomers were generated, which subsequently precipitated out of the solution and not further took part in any condensation reactions. As highlighted in section 1.5, such a phenomenon is counterproductive for a successful aldol trimerization. Another pivotal aspect warranting exploration is the impact of catalyst loadings. This factor wasn't exhaustively addressed in the current screening series and merits further investigation.

Table 3: Screened Lewis Acids in the polymerization of **13**

LA/H^+	Equ.	Solvent	Temperature	Precipitation	Residue
BF_3	0,1	DMSO	100	✓	✓
$SiCl_4$	2	EtOH	24	x	x
$SiCl_4$	2	Toluene	24	x	x
$SiCl_4$	0,1	oDCB	100	✓	✓
$TiCl_4$	6.2	oDCB	100	✓	x
VCl_3	0,1	oDCB	100	✓	✓
$FeCl_3$	0,1	oDCB	100	✓	✓
$ZrCl_4$	0,05	oDCB	100	✓	✓
$NbCl_5$	0,1	oDCB	100	✓	✓
$SnCl_4$/PTSAxH_2O	0.5/1	Pentanol	100	✓	x
$SbCl_5$	6	oDCB	100	✓	✓

The selection of *Brønsted* acids mirrored the approach taken for Lewis acids, drawing inspiration from literature examples that reported successful aldol trimerization reactions.[131–133] Additionally, the choice was influenced by instances where successful deprotection of the ketal group was documented.[134–137] The outcomes of these reactions are collated in Table 4.

A notable distinction when comparing the results of *Brønsted* acid-catalyzed reactions to those catalyzed by Lewis acids is the consistent correlation between precipitation and residue formation in the former. In other words, for the *Brønsted* acid trials, every instance of precipitation led to a final residue.

A closer examination of the results using PTSA underscores the pivotal role of the solvent in precipitate formation. Employing identical conditions in two solvents, oDCB and DMSO, only the former led to solid formation. The influence of the solvent in aldol trimerization has been previously highlighted by Amick and Scott.[99] While a direct explanation for this solvent-dependent behavior remains elusive, one can consider the polarizability of solvents, gauged by their refractive indices. At 20˚C, oDCB has a refractive index of 1.552, while DMSO's stands at 1.479.[54] This marginal difference might be pivotal in inducing precipitation in one solvent over the other. However, this hypothesis encounters a challenge when considering the precipitation observed in dichloroethane, which boasts an even lower refractive index (1.445)[54] than DMSO. Amick and Scott's discussion[99] posits that a solvent's high polarity should be beneficial for the aldol trimerization. Yet, the observed results hint that the reaction might not proceed as anticipated in highly polar solvents like DMSO.

An intriguing observation from the experiments is that the potency of the acid isn't the sole determinant for precipitation. Even a relatively weak acid like CSA can induce solid formation, underscoring the inherent acidity of monomer **14**. There are instances where reactions with higher acid strength did not result in precipitation. A case in point is the comparison between acetic acid and its trifluoro derivative. It's somewhat counterintuitive that the weaker acid (acetic

acid) leads to precipitate formation, while its stronger counterpart does not. This discrepancy is further influenced by the temperature variance in the two reactions.

The significance of temperature in the polymerization process became evident in trials involving PTSA and CSA. Initially set at 80 ˚C, the temperature was subsequently ramped up to 100 ˚C due to the absence of any precipitate. It was only post this increment that solid formation was observed. This underscores the criticality of maintaining elevated temperatures for the reaction.

Furthermore, while strong acids like hydrochloric acid and sulfuric acid did result in precipitation, the introduction of HCl gas did not yield any solid. This discrepancy can likely be attributed to the relatively cooler conditions in the latter reaction compared to the former.

Table 4: Screened *Brønsted* Acids in the polymerization of **13**

LA/H^+	Equ.	Solvent	Temperature	Precipitation	Residue
$HCl_{(g)}$		Dioxan	80	x	x
$HCl_{(g)}$		DMSO	80	x	x
PTSAxH_2O	0,1	Toluene	100	✓	✓
PTSAxH_2O	0,1	Dichloroethan	100	x	x
PTSAxH_2O	0,1	oDCB	100	✓	✓
PTSAxH_2O[1]	0,1	oDCB	80/100	✓	✓
PTSAxH_2O	0,1	DMSO	100	x	x
PTSAxH_2O/prop. Acid	3.5	oDCB	100	✓	✓
PPTS	0,1	oDCB	100	✓	✓
CSA	0,1	oDCB	100	✓	✓
CSA[1]	0,1	oDCB	80/100	✓	✓
MSA	0,1	oDCB	100	✓	✓
AcOH		-	100	✓	✓
TFA		-	80	x	x
H_2SO_4	3,7	oDCB	100	✓	✓
Conc. HCl		-	100	✓	✓

3.2.2 Characterizations

All samples underwent analysis using FT-IR spectroscopy and pXRAY diffraction, both of which offer invaluable insights regarding the success of the polymerization.

Powder X-Ray diffraction primarily provides data on the long-range order within a sample. This means it can be employed to ascertain the extent to which a crystalline network has been established. Given the objectives of this project, obtaining a crystalline structure is of paramount importance, making pXRAY diffraction a critical analytical tool.

[1] Reactions were initially kept at 80˚C for 10 days. Afterward, the reaction temperature was increased to 100 ˚C and kept for 5 days.

Conversely, infrared (IR) spectroscopy delves into the vibrational modes inherent to a material. In the context of this study, it becomes particularly useful in gauging the efficiency of the aldol trimerization. Specifically, by comparing the vibrational signals of the synthesized material to that of the monomer, one can deduce the extent of the reaction. A notable decrease in the C-H and C=O vibrational signals, when juxtaposed with the monomer, would be indicative of a successful bottom-up synthesis of the desired polybenzene network.

3.2.2.1 FT-IR

The FT-IR spectrum of monomer **14**, as depicted in Figure 15, showcases several prominent vibrational modes, each corresponding to specific molecular features:

- O-H Stretching (~3460 cm^{-1}): The broad signal centered around this wavenumber is indicative of O-H stretching. This could be due to residual moisture in the sample or, more intriguingly, a keto-enol tautomerization of the ketone functional groups. Keto-enol tautomerism is a dynamic equilibrium between a ketone (or aldehyde) and its isomeric enol form. This phenomenon is common in carbonyl compounds and can be detected by the presence of the O-H stretching vibration.
- C-H Vibration (~3000 cm^{-1}): The signal slightly below 3000 cm^{-1} arises from the C-H stretching vibration, a hallmark of hydrocarbons.
- Carbonyl Stretching (1705 cm^{-1}): The pronounced absorption at this wavenumber is characteristic of the C=O stretching vibration, a defining feature of carbonyl groups.
- Alpha-Beta Unsaturated Carbonyl Stretching (1605 cm^{-1}): The adjacent signal at around 1605 cm^{-1} can be ascribed to the stretching of an alpha-beta unsaturated carbonyl. This further supports the possibility of keto-enol tautomerization of the ketone functional groups.
- Complex Vibrational Modes (1500-400 cm^{-1}): The spectral region between these wavenumbers is populated with numerous distinct vibrational modes. These can be attributed to various molecular movements such as ring twisting, as well as asymmetric and symmetric stretching modes of the molecule. Given the complexity and overlap of these signals, a definitive assignment to specific molecular features or movements is challenging without further information.

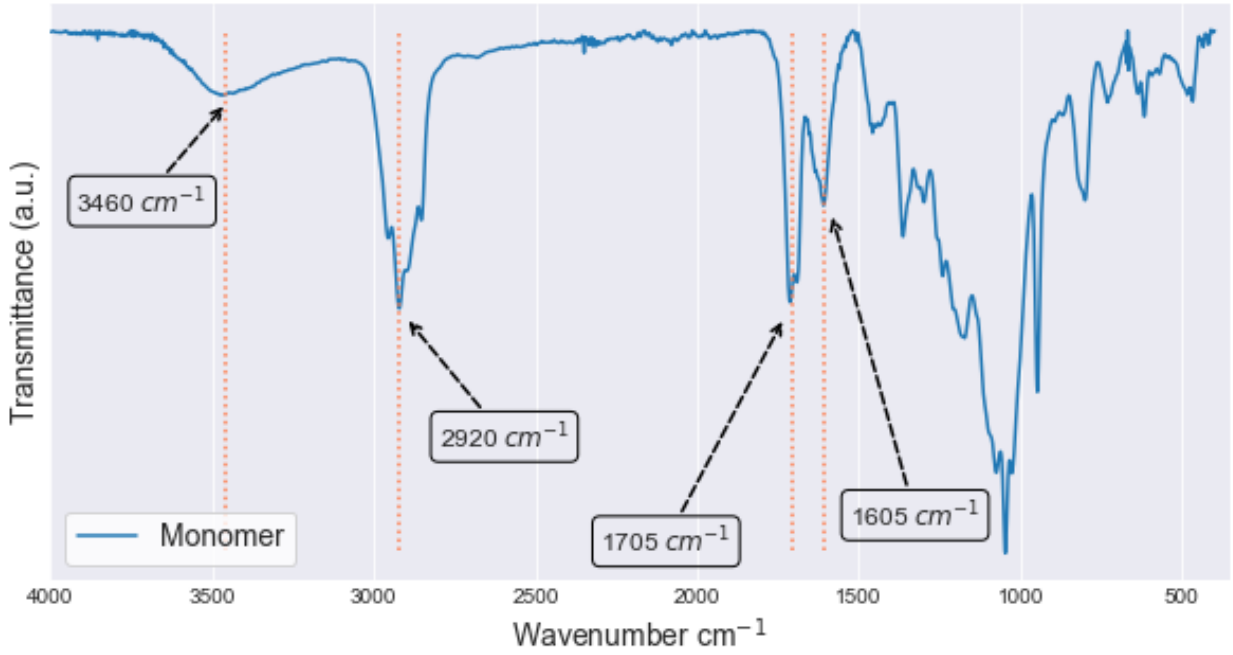

Figure 15: FT-IR spectrum of the monomer **14**

The FT-IR absorbance spectra for both *Brønsted* and Lewis acids are depicted in Figure 16 and Figure 17, respectively. respectively. Each spectrum is compared to the one of 14. Additionally, calculated absorption bands of the thermodynamically more stable 6.8[2] *D* allotrope are highlighted.[138] It's crucial to note that while comparing the spectra of the synthesized solid to the monomer, the transmittance units are arbitrary. The recorded signal was normalized based on the most pronounced vibrational mode. Consequently, the relative intensity among bands serves as the primary metric for assessing the transformation of functional groups.

The Lewis-catalyzed reactions exhibit a consistent trend across the samples. (Figure 16) Specifically, the intensity of the C-H stretching is reduced compared to the monomer in all instances, although it is not completely eliminated in most samples. Exceptions to this are $SiCl_4$ and $ZrCl_4$, where the signal is negligible, appearing just below a wavenumber of 2920 cm^{-1}. Concurrently, the relative intensity of the carbonyl vibration at 1705 cm^{-1} diminishes in all cases, indicating a loss of ketone functionalities in the synthesized samples. This observation is encouraging, as it suggests successful aldol condensation reactions.

A comparison of the obtained vibrational signals with the calculated ones reveals further insights. The vibrational mode at 1605 cm^{-1} is particularly noteworthy. In all samples, except the one catalyzed by $SbCl_5$, its relative intensity surpasses that of the carbonyl stretching. In the reaction catalyzed by the Niobium-halide, this vibration becomes the most intense one. However, it is important to recognize that no single experiment perfectly aligns with all the predicted signals, underscoring the complexity of the system under investigation.

Reactions catalyzed by $SbCl_5$ and BF_3 exhibit a pronounced baseline across a wide wavenumber range, indicative of the potential formation of a relatively amorphous material. Drawing a

definitive conclusion about which experiment yields the most favorable outcome is challenging based solely on this data. However, considering the reduction in carbonyl and C-H stretching intensities, coupled with the alignment to theoretical predictions, the reactions employing $SiCl_4$, VCl_3, and $NbCl_5$ appear to be promising candidates. Conversely, the experiments involving BF_3 and $SbCl_3$ do not seem to produce the anticipated products.

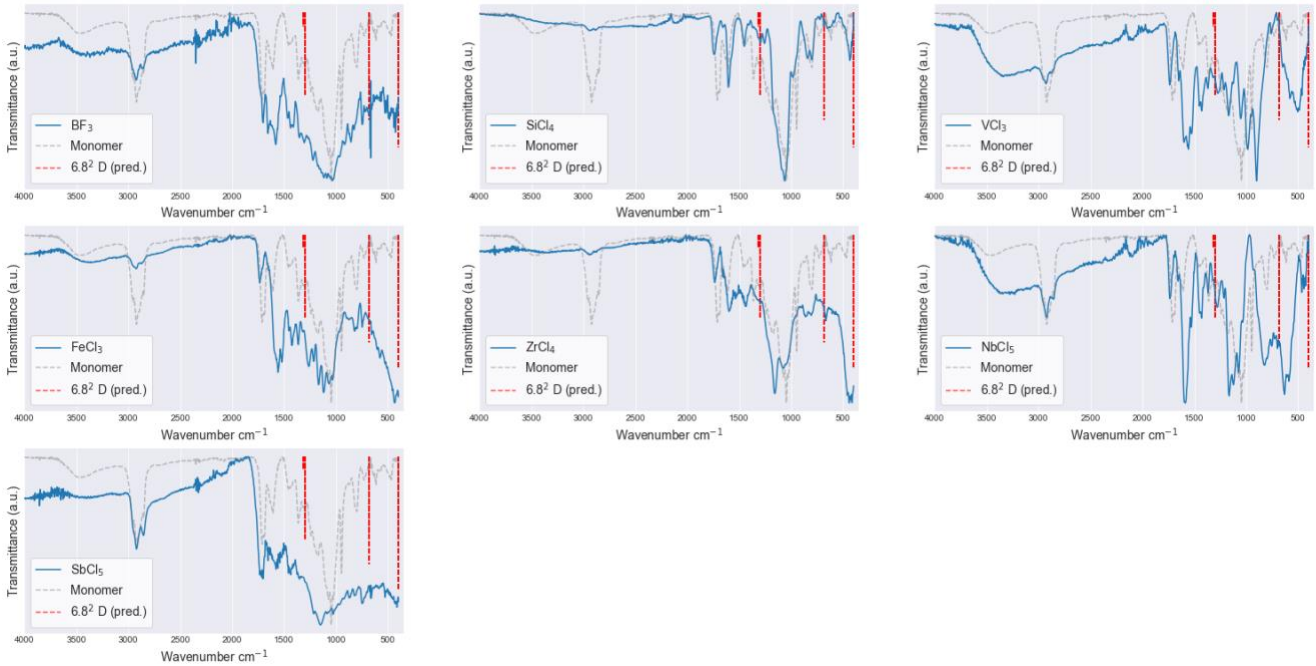

Figure 16: FT-IR spectra comparison of all polymerizations catalyzed by Lewis acids, placed alongside the spectra of monomer **14** and the anticipated 6.8² *D* allotrope.

Figure 17 presents the outcomes from the *Brønsted* acid-catalyzed reactions. A commonality across most reaction conditions is the diminished C-H vibration signal, with the notable exception of the PTSA/propionic acid-catalyzed reaction. Likewise, there's a consistent decrease in the carbonyl stretching at 1705 cm^{-1} across the samples, except in the reaction catalyzed by acetic acid. The behavior of the signal at 1605 cm^{-1} mirrors that observed in the Lewis acid-catalyzed reactions. Its relative intensity surpasses that of the carbonyl stretching in all samples, save for one.

Irrespective of the acidity of the specific sulfonic acid used, the resulting spectra exhibit striking similarities. Notably, the reactions catalyzed by PPTS and CSA at 100˚C appear almost indistinguishable. When juxtaposing the observed vibrational modes with the predicted ones, nearly all reactions display the band at 685 cm^{-1}. This stretching signal is conspicuously absent in the monomer's spectra. The reaction facilitated by sulfuric acid presents a pronounced baseline, suggesting the formation of amorphous carbon.

From the data presented, it appears that the sulfonic acid-catalyzed reactions hold the most promise. Conversely, employing concentrated acids, as well as acetic acid, doesn't seem to

produce the anticipated product. However, it's imperative to note that a conclusive statement cannot be drawn solely from the information provided.

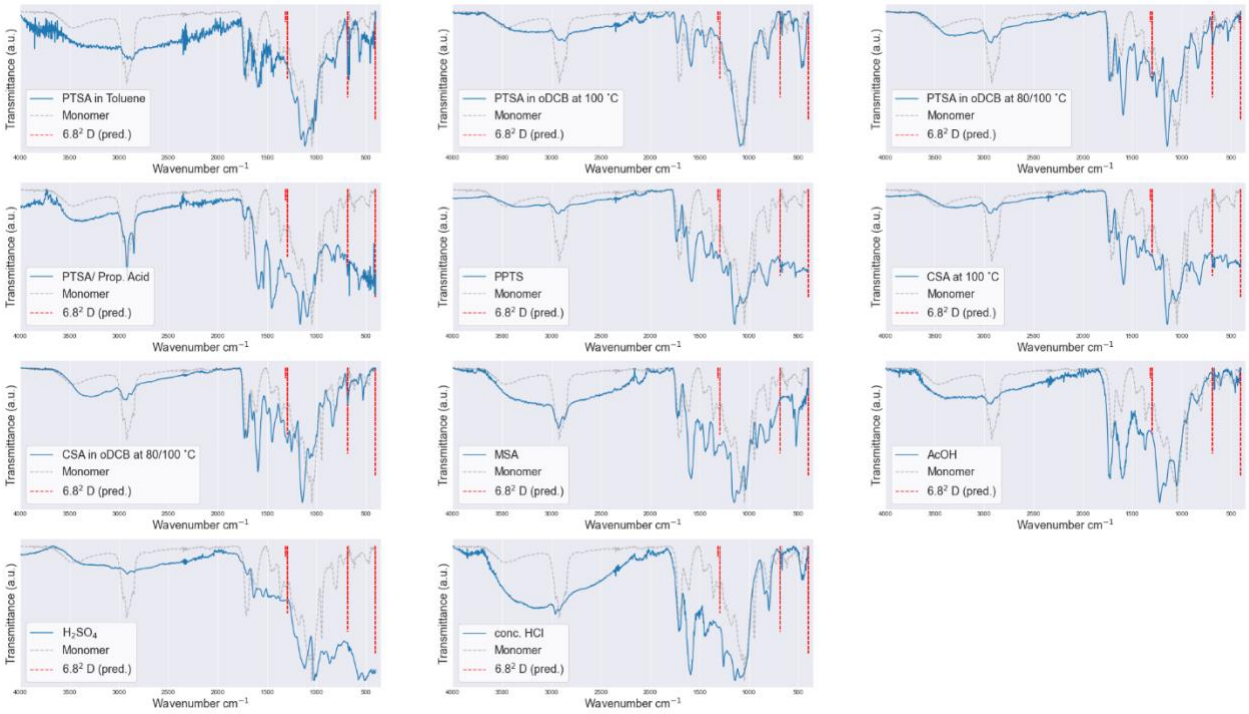

Figure 17: FT-IR spectra comparison of all polymerizations catalyzed by *Brønsted* acids, placed alongside the spectra of monomer **14** and the anticipated 6.8^2 *D* allotrope.

The findings presented here are indeed promising. While there are nuanced variations in the spectra across different experiments, an unmistakable trend is evident. Irrespective of the catalyst employed, there's a discernible reduction in the signals associated with both alkyl and carbonyl groups in the majority of samples. This is indicative of the anticipated aldol condensation taking place. Nonetheless, it's noteworthy that no single sample exhibits more than one vibrational mode that aligns with the theoretical predictions.

3.2.2.2 pXRD

The FT-IR spectra provided valuable insights into the transformation of functional groups within the synthesized powders. However, this method falls short in determining if a crystalline material was indeed produced. Such a determination can be effectively made using a pXRD (powder X-ray diffraction) experiment. Given that aldol trimerization has not been previously employed for COF synthesis, the presence of any peaks in the pXRD data can be deemed a success, as it would signify the formation of a crystalline framework.

Regrettably, not all samples were amenable to this analysis due to the insufficient quantity of the obtained powder. It's also essential to recognize that signal intensity in pXRD is contingent upon electron density. As such, even if the samples under investigation are crystalline, they might exhibit relatively subdued signal intensities. This challenge can be partially mitigated by adopting smaller angle increments and increasing sample loadings. However, given the limited availability

of the monomer and the desire to maximize test conditions, scaling up the experiments wasn't a viable option.

The resulting diffractograms are illustrated in Figure 18 and Figure 19. For clarity, the predicted pXRD patterns for both the 6.8^2 *D* and 6.8^2 *P* polymorphs are juxtaposed with the measured spectra of the monomer **14**.

The Lewis acid-catalyzed reactions present a specific challenge. These catalysts, often in the form of heterogeneous powders, are not soluble and typically remain undissolved during the workup. Consequently, it's anticipated that some residual peaks from these catalysts might be detected in the pXRD measurements.

Given the suboptimal signal-to-noise ratio in the data, any interpretations or conclusions drawn from the presented results should be approached with caution. A majority of the samples do not exhibit any discernible peaks, hinting at the formation of amorphous materials. The few samples that do display signals in the pXRD exhibit them at very low intensities. Notably, the signals characteristic of the monomer are absent in all other trials. This absence aligns with expectations, as any residual monomer would likely be eliminated during the workup process.

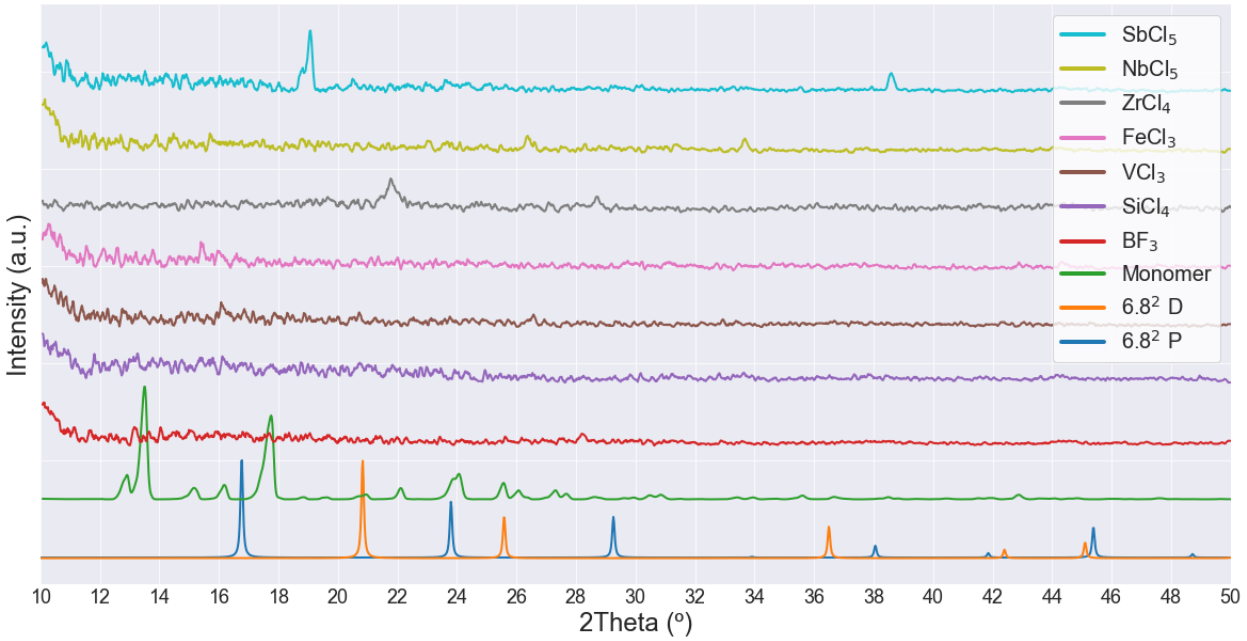

Figure 18: pXRD spectra of reactions catalyzed by Lewis acids, presented next to the spectra of monomer **14** and the predicted spectra for the target allotropes.

The solvent's influence is evident in the experiments involving PTSA in toluene and oDCB. While both conditions produce a peak in the pXRD data, they appear at distinct 2θ values. Intriguingly, the CSA-catalyzed reactions do not exhibit any peaks when initially held at 80˚C and subsequently raised to 100˚C. However, when maintained at 100˚C, two distinct signals emerge. The reaction facilitated by PPTS mirrors these diffraction peaks. Unexpectedly, analogous signals were observed in the experiment catalyzed by $NbCl_5$.

As previously highlighted, both CSA and PPTS are relatively weak acids. Their yielding consistent results is encouraging, implying that a similar supramolecular structure is formed when these weak acids are employed as catalysts. The appearance of the same signals in the $NbCl_5$-catalyzed reaction might be attributed to trace amounts of HCl released during the Lewis acid's hydrolysis, a consequence of water being liberated during the condensation process. However, challenging this hypothesis is the observation that under analogous conditions, $ZrCl_4$ - which possesses stability comparable to NbCl5 - does not produce the same peaks. This discrepancy warrants further investigation.

In the spectra obtained, two distinct patterns are discernible. The reactions catalyzed by $ZrCl_4$, concentrated HCl, and PTSA in oDCB exhibit a peak at a 2θ value of 21˚. In contrast, reactions facilitated by $NbCl_5$, CSA at 100˚C, and PPTS at 100˚C present two pronounced peaks at 2θ values of 26˚ and 34˚. Standing apart from these two clusters are the outcomes from reactions involving $SbCl_5$ and PTSA in toluene.

Notably, none of the spectra obtained align with the predicted patterns for either polymorph of polybenzene. To be more specific, the most intense peak anticipated for either polymorph is conspicuously absent across all measured spectra. Determining the structure based solely on these spectra is, regrettably, an unfeasible endeavor. Nevertheless, the results presented here underscore that the monomer **14** is capable of forming a network exhibiting at least some sort of crystallinity.

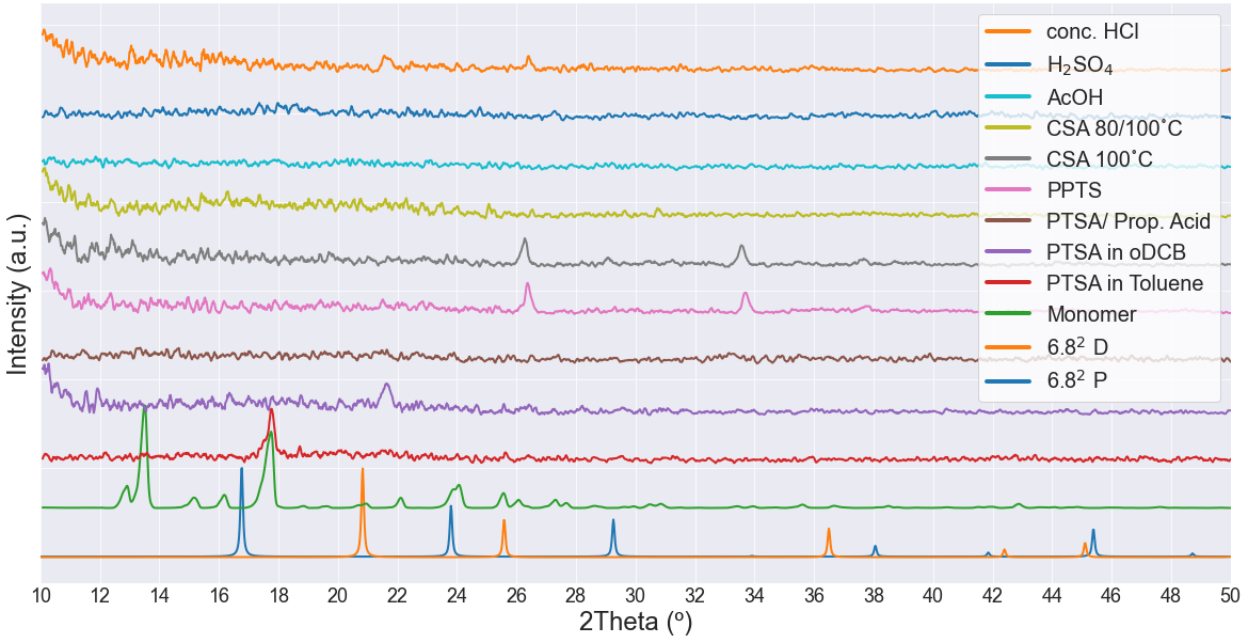

Figure 19: pXRD spectra of reactions catalyzed by *Brønsted* acids, presented next to the spectra of monomer 14 and the predicted spectra for the target allotropes.

4 Conclusion & Outlook

Although the primary objective of this study - the synthesis of a novel 3D carbon allotrope - was not achieved, the findings presented herein serve as a foundational step towards the intricate synthesis of such entities. A significant accomplishment of this research is the development of two distinct synthetic routes aimed at potential monomers for the realization of either the 6.8^2 *P* or 6.8^2 *D* polybenzene structures. Considerable optimization efforts were invested in the reactions undertaken, and crucially, both routes satisfy the imperative criterion of scalability. Each synthetic pathway possesses its unique set of merits and limitations, which are comprehensively discussed throughout this thesis.

The polymerization screenings underscore the inherent unpredictability of aldol trimerization. Drawing from reticular chemistry principles and existing literature, a comprehensive range of both Lewis and *Brønsted* acids were explored, alongside the effects of varying solvents and temperatures. An initial marker of success was identified in conditions that resulted in precipitation. These underscore the significance of elevated reaction temperatures and the pivotal role of the solvent in influencing outcomes.

FT-IR analysis of the derived powder samples revealed a consistent trend. Across all samples, there was a notable decrease in the relative intensity of the carbonyl vibration and a diminished signal corresponding to the C-H vibration when compared to the monomer. These observations suggest that the reaction is progressing as intended, leading to the formation of a carbon network.

However, pXRD analysis indicated that most of the samples were amorphous in nature. It's essential to highlight that the spectra were marred by a suboptimal signal-to-noise ratio, a consequence of limited sample quantities and the inherently low electron density of carbon. Intriguingly, a subset of samples exhibited a singular diffraction peak, hinting at the potential formation of a long-range ordered structure. Yet, none of these observed peaks aligned with the predicted patterns for either polymorph. Particularly compelling were the results derived from reactions utilizing the weaker acids, CSA and PPTS, as catalysts. Both exhibited identical diffraction signals, suggesting the formation of a consistent supramolecular network across these experiments. While the precise crystal structure of the procured polycrystalline samples remains elusive based on the current data, the emergence of consistent peaks across three independent experiments stands as a notable accomplishment.

Reflecting upon the research presented, it becomes evident just how formidable the challenge of realizing a novel carbon allotrope truly is. The journey ahead remains extensive. A clear impediment to progress is the limited availability of the monomer. As such, further refinements and optimizations of the more concise synthetic pathway B warrant consideration.

While this study offers preliminary insights into potentially promising conditions for procuring polycrystalline samples, discerning a definitive pattern in polymerization conditions that yield a promising product remains elusive. The employment of weak acids at elevated temperatures

emerges as a promising avenue. Yet, the peaks observed do not correspond to those anticipated for either modification of polybenzene.

Future endeavors should prioritize the replication of the results presented herein. Exploring polymerizations at even higher temperatures and experimenting with alternative high boiling solvents could provide valuable insights. Importantly, the synthetic sequence of route B presents an opportunity to incorporate varied protecting groups without necessitating a re-evaluation of subsequent reaction conditions. This flexibility could offer a more nuanced understanding of how the stability of a protecting group influences the aldol trimerization process en route to polybenzene.

5 Experimental Part

Unless otherwise stated, all manipulations of air and/or moisture-sensitive compounds were carried out in oven-dried glassware, under an atmosphere of N_2 or Ar. All solvents and reagents were purchased from Alfa Aesar, Spectrum Chemicals, Acros Organics, TCI America, and Sigma-Aldrich and were used as received unless otherwise noted. Zinc powder was activated by washing with 10% HCl and afterward dried under vacuum for 24 hours. Organic solvents were dried by passing through a column of alumina and were degassed by vigorous bubbling of N_2 or Ar through the solvent for 20 min. Flash column chromatography was performed on SiliCycle silica gel (particle size 40–63 µm). Thin layer chromatography was performed using SiliCycle silica gel 60 Å F-254 precoated plates (0.25 mm thick) and visualized by UV absorption. All ^{1}H and ^{13}C NMR spectra were recorded on Bruker AV-300, AVB-400, DRX-500, and AV-500 MHz spectrometers, and are referenced to residual solvent peaks ($CDCl_3$ ^{1}H NMR = 7.26 ppm, ^{13}C NMR = 77.16 ppm;). ESI mass spectrometry was performed on a Finnigan LTQFT (Thermo) spectrometer in positive ionization mode. FT-IR spectra were collected using a Bruker ALPHA Platinum ATR-FT-IR spectrometer with 40 scans averaging and a 4 cm^{-1} resolution. pXRD experiments were performed on a Rigaku MiniFlex 6G equipped with a HyPix-400 MF 2D detector. The scans were done at 5 degrees/sec increments and 0.01-degree step size, with a 2θ range of 10-50 degrees.

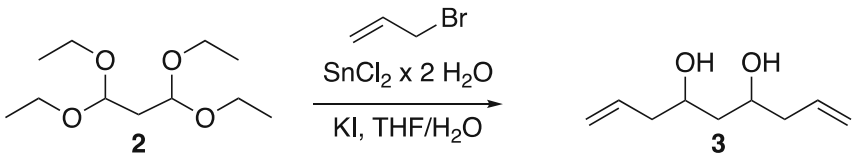

2 3

Nona-1,8-diene-4,6-diol (**3**) A 500 mL one necked Erlenmeyer flask was charged with 300 mL water and heated to 40˚C. Potassium iodine (45.20 g, 272.3 mmol), Tin(II)chloride dihydrate (61.45 g, 272.3 mmol) was added to the flask at once and stirred until the temperature reached 40˚C once again. 1,1,3,3-tetraethoxypropane (**2**) (20.00 g, 90.78 mmol, 3 M in THF) was added dropwise to reaction mixture. The suspension was stirred at 40˚C for 4h. The reaction mixture was extracted with CH_2Cl_2 (4 x 200 mL). The combined organic phases were washed with saturated aqueous Na_2SO_3 (300 mL) and saturated aqueous NaCl (300 mL), dried over $MgSO_4$ and concentrated on a rotary evaporator. Compound **3** (13.80 g, 88.32 mmol, 97%) was obtained as a light-yellow oil, which was used in the next step without further purification.

^{1}H NMR (400 MHz, $CDCl_3$) δ 5.88 – 5.70 (m, 2H), 5.18 – 5.01 (m, 4H), 4.03 – 3.82 (m, 2H), 3.17 (s, 2H), 2.36 – 2.11 (m, 4H), 1.67 – 1.35 (m, 2H) ppm.

^{13}C NMR (126 MHz, $CDCl_3$) δ 134.7, 134.3, 118.4, 118.4, 72.0, 68.4, 42.5, 42.1, 41.6, 41.4 ppm.

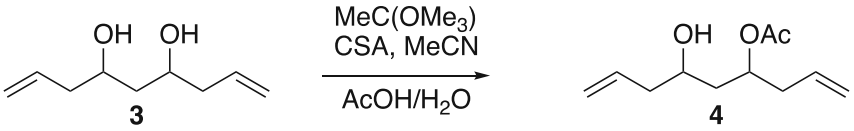

3 4

6-oxonona-1,8-dien-4-yl acetate (**4**) A 500 mL one necked round bottom flask was charged under air with Nona-1,8-diene-4,6-diol (**3**) (21.16 g, 135.3 mmol), 1,1,1-trimethoxyethane (32.54 g, 270,8 mmol) and CSA (1.572 g, 6.770 mmol) in Acetonitrile (60 mL). The reaction mixture was stirred at room temperature for 3 h. Afterward, the reaction mixture was hydrolyzed with Acetic Acid (60 mL, 50% in H_2O) and stirred overnight at 24 ˚C. The reaction mixture was mixed with saturated aqueous $NaHCO_3$ (200 ml) and extracted with DCM (3 x 200 mL). The combined organic phases were dried over $MgSO_4$ and concentrated on the rotary evaporator. Compound **4** (25.79 g, 130.1 mmol, 96%) was obtained as a yellow oil, which was used without further purification.

^{1}H NMR (400 MHz, $CDCl_3$) δ 5.89 – 5.66 (m, 2H), 5.17 – 5.03 (m, 5H), 3.78 – 3.52 (m, 1H), 2.43 (s, 1H), 2.38 – 2.13 (m, 4H), 2.05 (d, *J* = 14.6 Hz, 3H), 1.82 – 1.52 (m, 2H) ppm.

^{13}C NMR (126 MHz, $CDCl_3$) δ 172.0, 170.9, 134.8, 134.3, 133.5, 133.4, 118.4, 118.1, 118.0, 117.7, 71.6, 70.8, 68.4, 66.8, 42.0, 41.7, 41.5, 40.4, 39.3, 38.8, 21.3, 21.2 ppm.

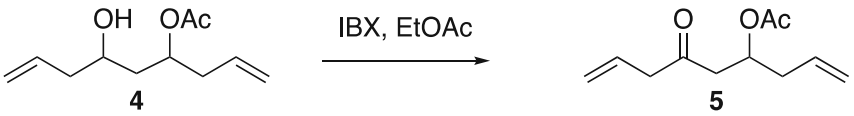

4 **5**

6-oxonona-1,8-dien-4-yl acetate (**5**) A 500 mL one necked flask with a reflux condenser was charged under air with **4** (13.76 g, 69.41 mmol) and IBX (23.32 g, 83.29 mmol) in EtOAc (200 mL). The reaction mixture was heated to 77˚C and stirred for 12 hours. The suspension was filtered, and the filtrate was flashed over a plug (Celite; EtOAc). The mixture was concentrated on a rotary evaporator, which yields **5** (13.49 g, 68.74 mmol, 99%) as a colorless oil, which was used without further purification.

^{1}H NMR (400 MHz, $CDCl_3$) δ 5.95 – 5.63 (m, 2H), 5.36 – 5.23 (m, 1H), 5.22 – 4.96 (m, 4H), 3.15 (d, *J* = 7.0 Hz, 2H), 2.82 – 2.54 (m, 2H), 2.43 – 2.25 (m, 2H), 1.98 (s, 3H) ppm.

^{13}C NMR (126 MHz, $CDCl_3$) δ 205.4, 170.3, 133.0, 119.3, 118.6, 69.2, 48.2, 45.6, 38.4, 21.1 ppm.

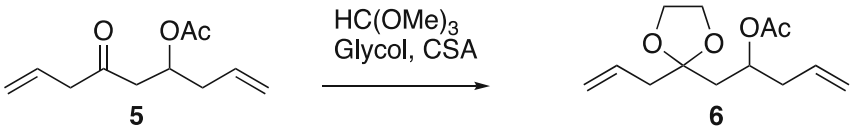

5 **6**

1-(2-allyl-1,3-dioxolan-2-yl)pent-4-en-2-yl acetate (**6**) A 250 ml one necked round bottom flask was charged under air with (**5**) (13.59 g, 69.24 mmol), Ethane-1,2-diol (85.95 g, 1385 mmol), Trimethoxymethane (29.39 g, 276.9 mmol), CSA (0.8041 g, 3.462 mmol). The reaction mixture was stirred at 24 ˚C for 4 hours and afterward was diluted with H_2O (100 mL) and CH_2Cl_2 (100 mL) and stirred for an additional 10 minutes at 24˚C. The reaction mixture was extracted with CH_2Cl_2 (4 x 150 mL). The combined organic phases were washed with saturated aqueous $NaHCO_3$ solution (100 mL), dried over $MgSO_4$, and concentrated on the rotary evaporator. Column chromatography (SiO_2; 25:3 hexane/EtOAc) yielded **6** (8.319 g, 34.62 mmol, 50%) as a colorless oil.

^{1}H NMR (400 MHz, $CDCl_3$) δ 5.74 (dddt, *J* = 23.0, 16.3, 10.6, 7.2 Hz, 2H), 5.18 (ddd, *J* = 8.2, 6.1, 3.5 Hz, 1H), 5.18 – 5.00 (m, 4H), 3.92 (dddd, *J* = 14.8, 9.5, 6.9, 4.8 Hz, 4H), 2.38 – 2.20 (m, 4H), 2.00 (s, 3H), 1.94 (dd, *J* = 15.1, 8.0 Hz, 1H), 1.82 (dd, *J* = 15.1, 3.5 Hz, 1H) ppm.

^{13}C NMR (126 MHz, $CDCl_3$) δ 170.6, 133.7, 133.1, 118.6, 118.0, 109.9, 69.1, 65.0, 42.5, 40.2, 39.9, 21.4 ppm.

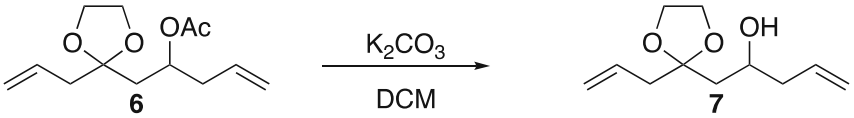

1-(2-allyl-1,3-dioxolan-2-yl)pent-4-en-2-ol (**7**) A one necked round bottom flask was charged under air with **6** (16.48 g, 68.56 mmol) and Potassium carbonate (113.7 g, 822.8 mmol) in Methanol (600 mL). The reaction mixture was stirred at 24 ˚C for 24 hours. The suspension was diluted with H_2O (200 mL) and extracted with CH_2Cl_2 (4x 300 mL). The combined organic phases were dried over $MgSO_4$ and concentrated on the rotary evaporator. Compound **7** (12.34 g, 62.22 mmol, 90%) was obtained as a colorless oil, which was used without further purification.

^{1}H NMR (400 MHz, $CDCl_3$) δ 5.79 (dddt, *J* = 21.0, 17.1, 14.3, 7.1 Hz, 2H), 5.15 – 5.02 (m, 4H), 4.08 – 3.89 (m, 5H), 3.35 (s, 1H), 2.40 (dd, *J* = 7.3, 1.4 Hz, 2H), 2.31 – 2.09 (m, 2H), 1.89 – 1.66 (m, 2H) ppm.

^{13}C NMR (126 MHz, $CDCl_3$) δ 134.9, 132.8, 118.8, 117.4, 111.4, 67.3, 65.1, 64.8, 42.2, 42.2, 41.8 ppm.

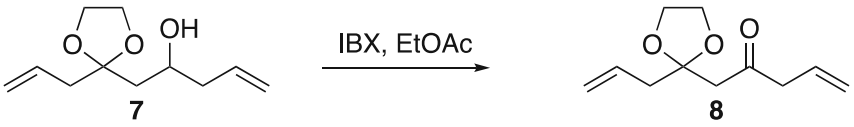

7 8

1-(2-allyl-1,3-dioxolan-2-yl)pent-4-en-2-one (**8**) A 500 mL one necked flask with a reflux condenser was charged under air with **7** (12.34 g, 62.22 mmol) and IBX (28.75 g, 102.7 mmol) in EtOAc (250 mL). The reaction mixture was heated to 77 ˚C and stirred for 24 hours. The suspension was filtered, and the filtrate was flashed over a plug (Celite, EtOAc). The mixture was concentrated on a rotary evaporator, which yields **8** (13.00 g, 66.21 mmol, ≥100%) as a colorless oil, that was used without further purification.

^{1}H NMR (400 MHz, $CDCl_3$) δ 5.98 – 5.72 (m, 2H), 5.21 – 5.06 (m, 4H), 3.97 (s, 4H), 3.25 (dt, *J* = 6.9, 1.4 Hz, 2H), 2.77 (s, 2H), 2.47 (d, *J* = 7.4 Hz, 2H) ppm.

^{13}C NMR (126 MHz, $CDCl_3$) δ 205.7, 196.9, 143.5, 132.7, 130.7, 119.2, 119.1, 118.9, 109.6, 109.3, 65.2, 65.2, 49.3, 49.1, 47.7, 42.9, 42.6, 18.4 ppm.

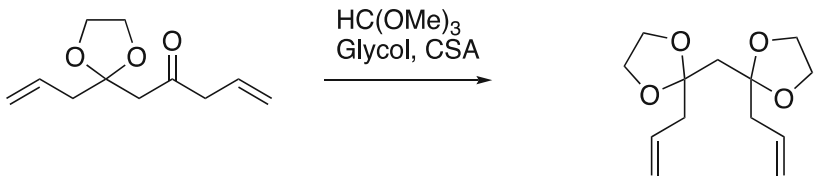

8 **9**

bis(2-allyl-1,3-dioxolan-2-yl)methane (**9**) A 250 mL one necked flask was charged under air with **8** (12.75 g, 64.97 mmol), Ethane-1,2-diol (80.65 g, 1299 mmol), Trimethoxymethane (27.58 g, 259.9 mmol), CSA (0.755 g, 3.248 mmol). The reaction mixture was stirred at 24˚C for 1,5 hours. The reaction mixture was diluted with H_2O (100 mL) and CH_2Cl_2 (100 mL) and stirred for additional 10 minutes at 24˚C. The reaction mixture was extracted with CH_2Cl_2 (4 x 200 mL. The combined organic layers were washed with saturated aqueous $NaHCO_3$ solution (100 mL), dried over $MgSO_4$, and concentrated on the rotary evaporator. Column chromatography (SiO_2; 9:1; hexane/EtOAc) yielded **9** (5.710 g, 23.78 mmol, 37%) as a colorless oil.

^{1}H NMR (400 MHz, $CDCl_3$) δ 5.82 (ddt, *J* = 17.3, 10.3, 7.1 Hz, 2H), 5.15 – 5.04 (m, 4H), 4.00 – 3.89 (m, 8H), 2.52 (dd, *J* = 7.1, 1.4 Hz, 4H), 1.97 (s, 2H) ppm.

^{13}C NMR (126 MHz, $CDCl_3$) δ 133.7, 133.6, 118.2, 109.6, 77.4, 64.8, 42.9, 42.4 ppm.

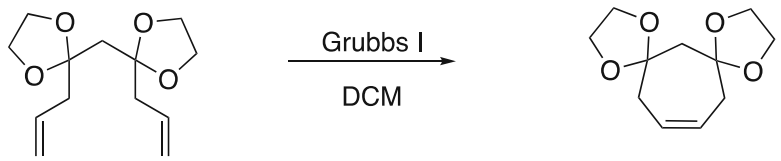

9 **10**

1,4,8,11-tetraoxadispiro[4.1.4^{7}.4^{5}]pentadec-13-ene (**10**) A dry 100 ml pressure round bottom flask, was charged under N_2 with **9** (3.300 g, 13.73 mmol) and 1,4,8,11-tetraoxadispiro[4.1.47.45]pentadec-13-ene (0.226 g, 0.275 mmol) in dry CH_2Cl_2 (50 mL). The reaction mixture was stirred at 60 ˚C for 24 hours. The reaction mixture was flashed over a plug (SiO_2; 4:1 hexane/EtOAc) and concentrated on the rotary evaporator. Column chromatography (SiO_2; 4:1 hexane/EtOAc) yielded **10** (2.460 g, 11.59 mmol, 84%) as a greyish oil.

^{1}H NMR (400 MHz, $CDCl_3$) δ 5.79 – 5.65 (m, 2H), 3.94 (s, 8H), 2.50 (d, *J* = 4.3 Hz, 4H), 2.19 (s, 2H) ppm.

^{13}C NMR (126 MHz, $CDCl_3$) δ 126.8, 108.2, 64.5, 49.0, 36.6 ppm.

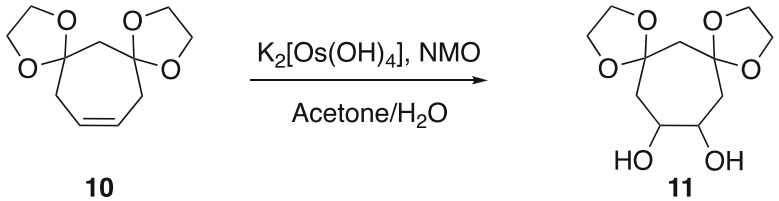

10 **11**

1,4,8,11-tetraoxadispiro[4.1.47.45]pentadecane-13,14-diol (**11**) A 100 ml flask was charged under air with **10** (2.723 g, 1.828 mmol) and Potassium osmate(VI) dihydrate (0.047 g, 0.128 mmol) in acetone (50 mL). To the reaction mixture, N-Methylmorpholine N-oxide (3.306 g, 28.22 mmol, 50% in H_2O) was added dropwise and the reaction mixture was stirred at 24 ˚C for 6 hours. Sodium dithionite (6.720 g, 28.22 mmol) was added to the reaction mixture at once and the suspension was stirred for 30 minutes. The reaction mixture was filtered over a celite cake and concentrated on a rotary evaporator. Column chromatography (SiO_2; 99:1hexane/MeOH) yielded **11** (2.432 g, 9.877 mmol, 77%) as a white solid.

^{1}H NMR (400 MHz, $CDCl_3$) δ 4.39 (dd, *J* = 7.2, 2.2 Hz, 1H), 4.25 (d, *J* = 4.9 Hz, 1H), 4.00 – 3.68 (m, 10H), 3.31 (s, 2H), 2.76 (dd, *J* = 13.9, 7.1 Hz, 1H), 2.05 (ddt, *J* = 10.6, 7.7, 3.5 Hz, 1H), 1.95 – 1.85 (m, 2H), 1.82 – 1.72 (m, 2H) ppm.

^{13}C NMR (126 MHz, $CDCl_3$) δ 107.4, 107.3, 81.5, 74.0, 64.7, 64.7, 63.8, 63.7, 62.1, 44.7, 42.6, 38.4 ppm.

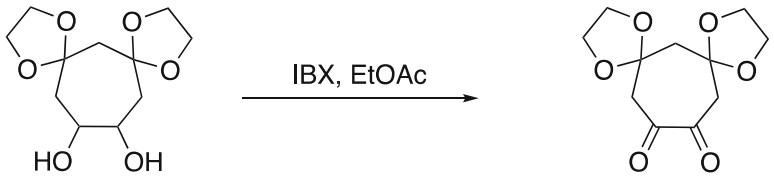

11 **12**

1,4,8,11-tetraoxadispiro[4.1.4^7.4^5]pentadecane-13,14-dione **12** A 100 mL one necked round bottom flask with a reflux condenser was charged under air with **11** (2.526 g, 10.26 mmol) and IBX (6.320 g, 22.57 mmol) in EtOAc (50 mL). The reaction mixture was heated to 77 ˚C and stirred for 24 hours. The suspension was filtered, and the filtrate was flashed over a plug (Celite, EtOAc) and concentrated on a rotary evaporator. Column chromatography (SiO_2; hexane/EtOAc 1:1) yields **12** (1.590 g, 6.565 mmol, 64%) as a beige solid.

^{1}H NMR (400 MHz, $CDCl_3$) δ 4.05 – 3.92 (m, 8H), 3.05 (s, 4H), 2.36 (s, 2H) ppm.

^{13}C NMR (126 MHz, $CDCl_3$) δ 195.6, 105.3, 64.9, 64.9, 48.9, 47.8 ppm.

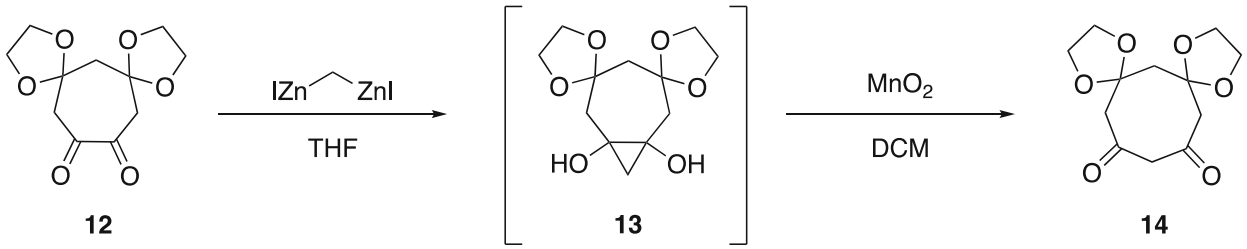

1,4,8,11-tetraoxadispiro[4.1.4^7.5^5]hexadecane-13,15-dione **14** A 10 ml microwave vial was charged under N_2 with **12** (0.169 g, 0.699 mmol) in dry Tetrahydrofuran (5.6 mL). Freshly prepared Simmons-Smith reagent (3.15 mL, 0,945 mmol, 0.3 M in THF) reagent was added at once and the vial was shaken for 5 minutes at 24 ˚C. The reaction mixture was poured into a mixture of DCM (100mL) and saturated aqueous NH_4Cl (100 ml) and stirred for 30 minutes. The suspension was extracted with CH_2Cl_2 (4x100 mL). The combined organic phases were dried over $MgSO_4$ and concentrated on a rotary evaporator.

A 100 mL one-necked round bottom flask was charged with the crude solid of **13** and Manganese(IV)oxide (2.584 g, 29.73 mmol) in CH_2Cl_2 (25 mL). The reaction mixture was stirred at 24 ˚C for 1,5 hours. The reaction mixture was filtered over a pad of celite and the filtrate was concentrated on a rotary evaporator. Column chromatography (SiO_2; 2:3 hexane/EtOAc) yielded **14** (52.2 mg, 0.2037 mmol, 29%) as a white solid.

^{1}H NMR (500 MHz, $CDCl_3$) δ 3.97 (s, 8H), 3.79 (s, 2H), 2.94 (s, 4H), 2.22 (s, 2H) ppm.

^{13}C NMR (126 MHz, $CDCl_3$) δ 198.4, 105.5, 64.5, 60.0, 52.6, 47.7 ppm.

HRMS (EI-TOF) m/z: $[C_{12}H_{18}O_6]^+$ calcd. $[C_{12}H_{18}O_6]$256.0947: found 256.0948.

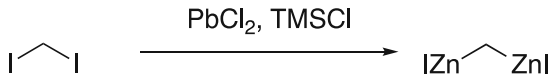

Bis(idozincomethane) A 10 mL dry microwave vial was charged under N_2 with activated Zinc dust (1.440 g, 22.03 mmol), Lead(II)-chloride (0.100 g, 0.360 mmol) and Chlorotri(methyl)silane (0.399 g, 3.673 mmol) in dry Tetrahydrofuran (6 mL). The reaction mixture was sonicated for 30 minutes at 24˚C. Diiodomethane (0.160 g, 0.597 mmol) was added at once and the reaction mixture was sonicated for another 30 minutes at 24˚C. Afterward, diiodomethane (1.000 g, 3.734 mmol) was added dropwise to the mixture over 30 minutes at 24˚C and the suspension was stirred for 12 hours.

The concentration of the mixture was determined via a Benchmark reaction with Benzaldehyde. An exemplary procedure to determine the concentration is described here. A dry 10 mL microwave vial was charged under N_2 with Benzaldehyde (35.4 mg, 0.334 mmol) and the freshly prepared bis(idozincomethane) solution (0,1 mL). The reaction mixture was stirred at 24 ˚C for 2h. The concertation of the bis(idozincomethane) solution was determined by NMR analysis. More specifically by the relative integration of the Benzaldehyde and Styrene signals.

$$c_{\text{Bis(idozincomethane)}} = \frac{n_{Benzaldehyde}}{\int_{Benzaldehyde+Styrene}} \cdot \frac{\int_{Styrene}}{V_{\text{Bis(idozincomethane)}\ h}}$$

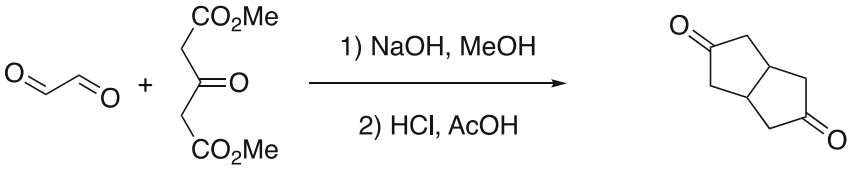

15 **16** **17**

tetrahydropentalene-2,5(1H,3H)-dione **17** A three-necked round bottom flask with a reflux condenser and a dropping funnel was charged under air with finely powdered Sodium hydroxide (6.500 g, 162.5 mmol) in dry methanol (90 mL). The reaction mixture was cooled using an ice bath and Dimethyl-1,3-acetonedicarboxylate (**16**) (27.74 g, 159.3 mmol) was added dropwise over a period of 2 hours. The ice bath was removed, and the reaction mixture was heated to 65 ˚C for 1 hour. Glyoxal (**15**)(11,56 g, 199,1 mmol, 40% in H_2O) was added dropwise over a period of 90 minutes. Afterward, the heating was removed, and the solution was stirred at 24 ˚C for 12 hours. The suspension was filtered, and the filtrate was washed with methanol (70 mL) to give a beige solid.

A 250 ml one necked flask with a reflux condenser and a bubbler was charged with the crude solid in 1 M HCl (70 mL) and Acetic acid (7mL). The reaction mixture was heated to 100 ˚C and stirred for 18 hours. The solution was extracted with $CHCl_3$ (3x 50 mL). The combined organic phases were washed with saturated aqueous $NaHCO_3$ solution (100 mL) and concentrated on a rotary evaporator. Recrystallization (2:1 hexane:EtOAc) gave **17** (5,535, 40,06 mmol, 50 %) as a white solid.

^{1}H NMR (400 MHz, $CDCl_3$) δ 3.03 (dddd, *J* = 13.5, 8.7, 6.7, 4.8 Hz, 2H), 2.63 – 2.50 (m, 4H), 2.20 – 2.07 (m, 4H) ppm.

^{13}C NMR (126 MHz, $CDCl_3$) δ 218.0, 43.8, 36.6 ppm.

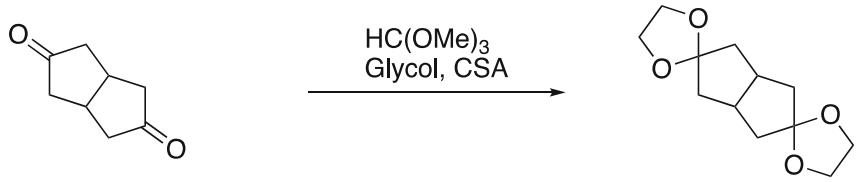

17 **23**

tetrahydro-1'*H*,3'*H*-dispiro[[1,3]dioxolane-2,2'-pentalene-5',2''-[1,3]dioxolane] **23** A 10 mL one necked round bottom flask was charged under air with **17** (97.9 mg, 0.709 mmol), Ethane-1,2-diol (1.759 g, 28.34 mmol), Trimethoxymethane (0.602 g, 5.668 mmol), CSA (8.2 mg, 0.035 mmol). The reaction mixture was stirred at 24˚C for 1,5 hours. The reaction mixture was diluted with H_2O (5 mL) and CH_2Cl_2 (5 mL) and stirred for additional 10 minutes at 24˚C. The reaction mixture was extracted with CH_2Cl_2 (4 x 50 mL). The combined organic layers were washed with saturated aqueous $NaHCO_3$ (50 mL), dried over $MgSO_4$ and concentrated on the rotary evaporator. Column chromatography (SiO_2; 17:3; hexane/EtOAc) yielded **23** (0.128 g, 0.566 mmol, 80%) as a white solid.

^{1}H NMR (400 MHz, $CDCl_3$) δ 3.71 (s, 8H), 2.41 (h, *J* = 8.3 Hz, 2H), 1.79 (dd, *J* = 13.6, 7.4 Hz, 4H), 1.53 (dd, *J* = 13.3, 5.5 Hz, 4H) ppm.

^{13}C NMR (126 MHz, $CDCl_3$) δ 118.4, 64.7, 64.3, 44.5, 42.6, 37.1 ppm.

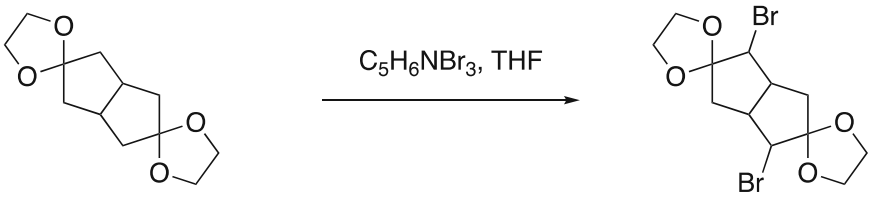

23 **24**

1',4'-dibromotetrahydro-1'*H*,3'*H*-dispiro[[1,3]dioxolane-2,2'-pentalene-5',2''-[1,3]dioxolane] **24**
A dry 50 ml Schlenk flask was charged under N_2 with **23** (0.850 g, 3.754 mmol) in Tetrahydrofuran (20 mL). The reaction mixture was cooled to -78 ˚C. Pyridinium perbromide (2.642 g, 8.260 mmol) was added at once and the reaction mixture was stirred for 1h. The reaction mixture was mixed with H_2O (100 mL) and extracted with CH_2Cl_2 (3 x 50 mL). The combined organic phases were dried over $MgSO_4$ and concentrated on the rotary evaporator. Recrystallization (Methanol) yielded **24** (0,447 g, 1,163 mmol, 31%) as a white solid.

^{1}H NMR (400 MHz, $CDCl_3$) δ 4.17 – 3.91 (m, 10H), 3.02 – 2.88 (m, 2H), 2.40 – 2.26 (m, 2H), 1.89 – 1.75 (m, 2H) ppm.

^{13}C NMR (101 MHz, $CDCl_3$) δ 115.7, 66.0, 65.7, 58.5, 45.7, 37.1 ppm.

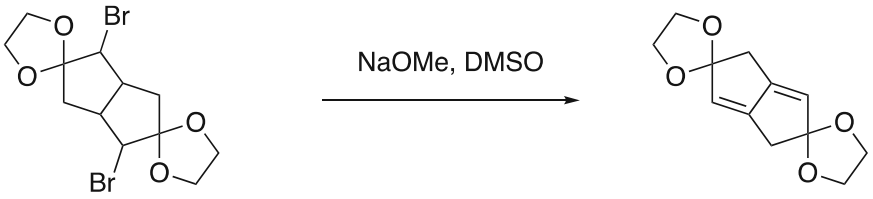

24 **18**

1'*H*,4'*H*-dispiro[[1,3]dioxolane-2,2'-pentalene-5',2''-[1,3]dioxolane] **18** A 6 mL vial was charged under N_2 with **24** (25.7 mg, 0.070 mmol) and Sodium methoxide (21.7 mg, 0.402 mmol) in Dimethylsulfoxide (1mL). The reaction mixture was stirred at 70 ˚C for 2 hours. The reaction mixture was diluted with saturated aqueous NH_4Cl solution (10 mL) and extracted with CH_2Cl_2 (3x25 mL). The combined organic phases were dried over $MgSO_4$ and concentrated on the rotary evaporator. Column chromatography (SiO_2; 2:1 hexane/EtOAc) yielded **18** (3.1 mg, 0.014 mmol, 20%) as a white solid.

^{1}H NMR (400 MHz, $CDCl_3$) δ 5.46 (s, 2H), 3.94 (s, 8H), 2.68 (s, 4H) ppm.

^{13}C NMR (101 MHz, $CDCl_3$) δ 153.2, 122.4, 121.3, 64.9, 37.1 ppm.

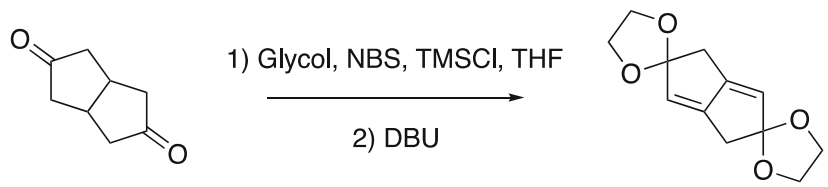

17 **18**

1'*H*,4'*H*-dispiro[[1,3]dioxolane-2,2'-pentalene-5',2''-[1,3]dioxolane] **18** A 25 mL Schlenk flask was charged under N_2 with **17** (4.979 g, 36.03mmol), Ethane-1,2-diol (35.784 g, 576.5mol) in dry Tetrahydrofuran (72 mL). The reaction mixture was cooled to -78 ˚C and NBS (14.1088 g, 79.269 mmol), Chlorotri(methyl)silane (11.74 g, 108.1 mmol) were added. The reaction mixture was stirred at 24 ˚C for 3 hours. The reaction mixture was diluted with saturated aqueous $NaHCO_3$ (150 mL) and extracted with CH_2Cl_2 (4 x 150 mL). The combined organic phases were dried over $MgSO_4$ and concentrated on the rotary evaporator.

A 25 mL one-necked round bottom flask was charged with the crude solid and DBU (16.46 g, 108.1 mmol). The reaction mixture was heated to 120 ˚C and stirred for 72 hours. The reaction mixture was diluted with H_2O (200 mL) and extracted with CH_2Cl_2(3 x 300 mL). The combined organic phases were dried over $MgSO_4$ and concentrated on a rotary evaporator. Column chromatography (SiO_2; 2:1 hexane/EtOAc) yielded **18** (1.803 g, 8.112 mmol, 23%) as a white solid.

^{1}H NMR (400 MHz, $CDCl_3$) δ 5.46 (s, 2H), 3.94 (s, 8H), 2.68 (s, 4H) ppm.

^{13}C NMR (101 MHz, $CDCl_3$) δ 153.2, 122.4, 121.3, 64.9, 37.1 ppm.

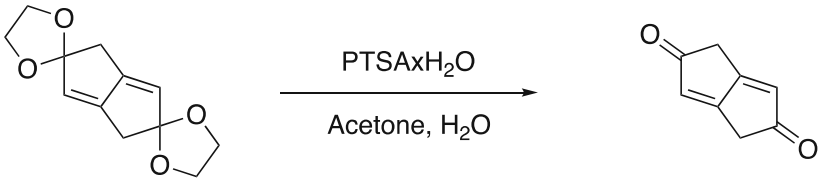

18 **19**

1'*H*,4'*H*-dispiro[[1,3]dioxolane-2,2'-pentalene-5',2''-[1,3]dioxolane] **19** A 25 ml flask was was charged under air with **18** (0.110 g, 0.494 mmol) and PTSAxH_2O (7.9 mg, 0.042 mmol) in acetone (6.5 mL). The reaction mixture was stirred at 24 ˚C for 36 hours. H_2O (0.300 g, 16.62 mmol) was added and the reaction mixture was stirred for an additional 24 hours. The reaction mixture was diluted with saturated aqueous $NaHCO_3$ solution (30 mL) and extracted with CH_2Cl_2 (4x50 mL). The combined organic phases were dried over $MgSO_4$ and concentrated on a rotary evaporator. Column Chromatography (SiO_2; 2:1 hexane/EtOAc) yielded **19** (0.056 g, 0.418 mmol, 85%) as a white solid.

^{1}H NMR (400 MHz, $CDCl_3$) δ 6.32 (s, 2H), 3.24 (s, 4H) ppm.

^{13}C NMR (126 MHz, $CDCl_3$) δ 202.5, 171.8, 127.7, 36.0 ppm.

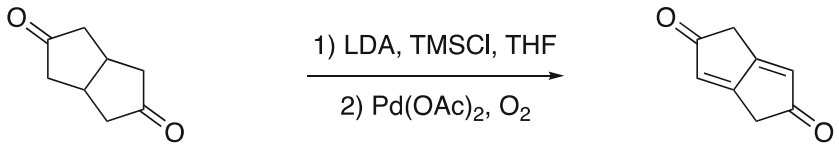

17 **19**

1'*H*,4'*H*-dispiro[[1,3]dioxolane-2,2'-pentalene-5',2''-[1,3]dioxolane] **19** A dry 10 ml Schlenk flask was charged under N_2 with **17** (0.204 g, 1.474 mmol) and Chlorotri(methyl)silane (0.416 g, 3.831 mmol) in dry Tetrahydrofuran (4 mL). The reaction mixture was cooled to -78˚C and LDA solution (1,73 mL, 3,46 mmol, 2 M in THF/heptane/ethylbenzene) was added dropwise and stirred at -78˚C for 1 hour. Afterward, the reaction mixture was warmed to 24 ˚C and stirred for 12 hours. The reaction mixture was concentrated on a rotary evaporator and the solid residue was taken up in saturated aqueous $NaHCO_3$ solution (30 mL) and extracted with hexane (4x25 mL). The combined organic phases were dried over $MgSO_4$ and concentrated on a rotary evaporator.

A 50 mL Schlenk flask was charged under O_2 with the crude oil and Palladium(II) acetate (0.076g, 0.336 mmol) in Dimethylsulfoxide (11 mL). The reaction mixture was stirred at 24 ˚C for 12 hours. The reaction mixture was diluted with H_2O (20 mL) and extracted with EtOAc (4x 25 mL). The combined organic phases were dried over $MgSO_4$ and concentrated on a rotary evaporator. Column chromatography (SiO_2; 13:9 Hexanes/EtOAc) yielded **19** (0.007 g, 0.052 mmol, 3%) as a white solid.

^{1}H NMR (400 MHz, $CDCl_3$) δ 6.32 (s, 2H), 3.24 (s, 4H) ppm.

^{13}C NMR (126 MHz, $CDCl_3$) δ 202.5, 171.8, 127.7, 36.0 ppm.

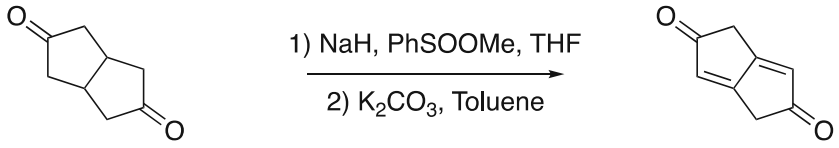

17 **19**

1'*H*,4'*H*-dispiro[[1,3]dioxolane-2,2'-pentalene-5',2''-[1,3]dioxolane] **19:** A dry 10 mL Schlenk flask was charged under N_2 with Sodiumhydride (0.373 g, 9.316 mmol, 60% in mineral oil) and methyl benzenesulphinate (0.562 g, 3.600 mmol) in dry Tetrahydrofuran (1.5 ml) To the reaction mixture **17** (0,212 g, 1,532 mmol, in 2 mL dry THF) was added dropwise at 24 ˚C. After stirring at 24 ˚C for 12 hours the reaction mixture was quenched with acetic acid (50 mL, 10% in H_2O) and extracted with CH_2Cl_2 (4x30 mL). The combined organic phases were dried over $MgSO_4$ and concentrated on a rotary evaporator. The crude mixture was flashed over a plug (SiO_2; 1:1 hexane/EtOAc) and concentrated on a rotary evaporator.

A 25 ml flask was charged under air with the crude solid and Sodiumbicarbonate (0.810 g, 9.642 mmol) in Toluene (5 mL). The reaction mixture was heated to 110 ˚C for 1,5 hours. Afterward, filtration was performed, and the filter cake was washed with toluene (25 mL). The organic solvent was reduced on a rotary evaporator. Column chromatography (SiO_2; 3:2 Hexane/EtOAc) yielded **19** (5,8 mg, 0,0432 mmol, 3%) as a white solid.

^{1}H NMR (400 MHz, $CDCl_3$) δ 6.32 (s, 2H), 3.24 (s, 4H) ppm.

^{13}C NMR (126 MHz, $CDCl_3$) δ 202.5, 171.8, 127.7, 36.0 ppm.

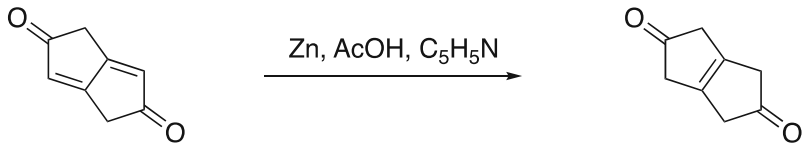

19 **20**

4,6-dihydropentalene-2,5(1*H*,3*H*)-dione **20** A 8 ml vial was charged under air with **19:** (46.9 mg, 0.350 mmol), Zinc (0.274 g, 4.194 mmol) and pyridine (1.031 g, 13.032mmol) in THF (1.05 mL). The reaction mixture was cooled to 0 ˚C and acetic acid (0,4091 g, 6,813mmol) was added dropwise to the reaction mixture. Afterward, the reaction mixture was stirred at 24 ˚C for 1 hour. The reaction mixture was diluted with 2M H_2SO_4 (10 mL) and extracted with CH_2Cl_2 (4 x50 mL). The combined organic phases were dried over $MgSO_4$ and reduced on the rotary evaporator. Compound **20** (44,3 mg, 0,325 mmol, 94 %) was obtained as a beige solid, without further purification.

^{1}H NMR (400 MHz, $CDCl_3$) δ 2.99 (s, 8H) ppm.

^{13}C NMR (101 MHz, $CDCl_3$) δ 214.4, 138.5, 42.3 ppm.

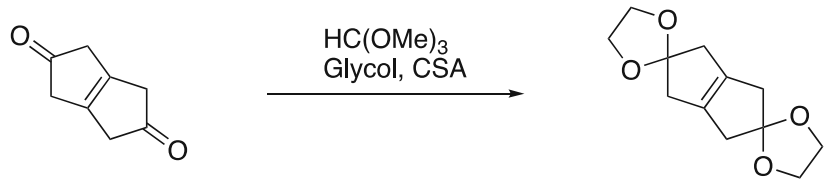

20 **21**

4',6'-dihydro-1'*H*,3'*H*-dispiro[[1,3]dioxolane-2,2'-pentalene-5',2''-[1,3]dioxolane] **21:** A 8 mL vial was charged under air with **20** (0.0172 mg, 0.126mmol), Ethane-1,2-diol (1.2466 g, 20.083 mmol), Trimethoxymethane (0.134 g, 1.264 mmol), CSA (1.5 mg, 0.007 mmol). The reaction mixture was stirred at room temperature for 3 hours. The reaction mixture was diluted with saturated aqueous $NaHCO_3$ solution (10 mL) and extracted with CH_2Cl_2 (4 x 50 mL). The combined organic layers were dried over $MgSO_4$ and concentrated on the rotary evaporator. Column chromatography (SiO_2: 4:1; hexane/EtOAc) yielded **21** (0.012 g, 0.052 mmol, 41%) as a white solid.

^{1}H NMR (400 MHz, $CDCl_3$) δ 3.95 (s, 8H), 2.53 (s, 8H) ppm.

^{13}C NMR (101 MHz, $CDCl_3$) δ 137.5, 120.2, 64.4, 42.5 ppm.

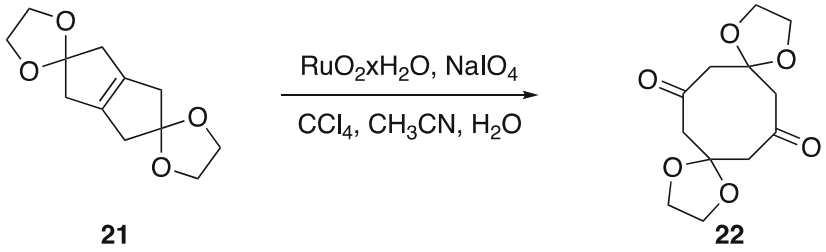

21 **22**

1,4,10,13-tetraoxadispiro[4.3.4^{9}.3^{5}]hexadecane-7,15-dione **22:** A 8 mL vial was charged under air with **21** (0.012 g, 0.052 mmol), Sodium periodate (0.047 g, 0.219 mmol), Ruthenium(IV) oxide hydrate (0.157 mg, 0.001 mmol) in CCl_4 (0.26 ml), CH_3CN (0.26 mL) and H_2O (0.37 mL). The reaction mixture was stirred at 24 ˚C for 0.5 hours. The reaction mixture was diluted with H_2O (10 mL) and extracted with CH_2Cl_2 (4 x 20 mL). The combined organic layers were dried over $MgSO_4$ and concentrated on the rotary evaporator. Compund **22** (0,018 g, 0,068 mmol, ≥100 %) was obtained as a brown solid without further purification.

^{1}H NMR (400 MHz, $CDCl_3$) δ 4.04 (s, 8H), 3.01 (s, 8H) ppm.

^{13}C NMR (101 MHz, $CDCl_3$) δ 203.1, 105.0, 64.9, 52.9 ppm.

HRMS (EI-TOF) m/z: $[C_{12}H_{18}O_6]^+$ calcd. $[C_{12}H_{18}O_6]$ 256.0947: found 256.0947.

General Procedure Polymerizations:

A dry 10 mL microwave vial under N_2 was charged with **14** and LA/H^+ in a solvent (0.1 M). The reaction mixture was heated without stirring for 14 days. The reaction was worked up by washing the precipitate with approximately 5 mL of each solvent followed by centrifugation (10000 rpm 3 min.): Dimethylsulfoxide, Dimethylformamide, Acetonitrile, Toluene, CHCl3, DCM, EtOAc, Methanol, Diethylether, Hexanes, Acetone. If a residual black solid was obtained it was dried under reduced pressure for 24 hours.

Table 5: Reaction conditions of all polymerization attempts

14 (mg)	**14** (mmol)	LA/H^+	LA/H^+ (mg)	LA/H^+ (mmol)	Equ.	Solvent	Volume (mL)	Temperature (˚C)
11.0	0.043	$SiCl_4$	14.6	0.086	2	EtOH	0.11	24
11.5	0.045	$SiCl_4$	14.6	0.086	2	Toluene	0.12	24
11.5	0.045	$PTSAxH_2O$	0.8	0.004	0,1	Toluene	0.12	100
10.5	0.041	$PTSAxH_2O$	0.8	0.004	0,1	Dichloroethan	0.10	100
20.0	0.078	$PTSAxH_2O$	1.2	0.006	0,1	oDCB	0.78	100
11.0	0.043	AcOH				-	0.12	100
32.9	0.128	TFA				-	1.00	80
15.0	0.059	$ZrCl_4$	1.0	0.004	0,05	oDCB	0.58	100
15.0	0.059	BBr_3	28.0	0.112	2	oDCB	0.50	100
20.6	0.080	$PTSAxH_2O$/prop. Acid	53.5/21.0	0.281/0.283	3.5	oDCB	0.30	100
20.7	0.081	$TiCl_4$	95.0	0.501	6.2	oDCB	2.50	100
18.7	0.073	$SnCl_4/PTSAxH_2O$	10.0/13.9	0.038/0.073	0.5/1	Pentanol	0.72	100
15.2	0.059	H_2SO_4	366.0	3.732	3,7	oDCB	0.60	100
29.0	0.113	PPTS	3.0	0.012	0,1	oDCB	1.14	100
23.6	0.092	CSA	2.2	0.009	0,1	oDCB	0.92	100
15.0	0.059	$SbCl_5$	94.4	0.316	6	oDCB	0.59	100
16.2	0.063	$FeCl_3$	1.0	0.006	0,1	oDCB	0.63	100
29.1	0.114	$HCl_{(g)}$				Dioxan	2.00	80
28.1	0.110	$HCl_{(g)}$				DMSO	2.00	80
20.0	0.078	Conc. HCl				-	0.78	100
28.2	0.110	$PTSAxH_2O$	2.1	0.011	0,1	DMSO	1.10	100
25.6	0.100	BF_3	0.7	0.010	0,1	DMSO	1.00	100
19.5	0.076	$SiCl_4$	1.3	0.008	0,1	oDCB	1.00	100
9.7	0.038	$NbCl_5$	1.0	0.004	0,1	oDCB	1.00	100
18.8	0.073	VCl_3	1.2	0.008	0,1	oDCB	1.00	100
26.2	0.102	MSA	1.0	0.010	0,1	oDCB	1.02	100
14.7	0.057	CSA	1.4	0.006	0,1	oDCB	0.57	80/100[2]
12.3	0.048	$PTSAxH_2O$	0.9	0.005	0,1	oDCB	0.48	80/100[2]

[2] Reactions were kept at 80 ˚C for 10 days. After that time the reaction temperature was increased to 100˚C for an additional 5 days.

Table 6: Precipitation results of all polymerization attempts

LA/H^+	Equ.	Solvent	Temperature (˚C)	Precipitation	Residue
$SiCl_4$	2	EtOH	24	x	x
$SiCl_4$	2	Toluene	24	x	x
$PTSAxH_2O$	0,1	Toluene	100	✓	✓
$PTSAxH_2O$	0,1	Dichloroethan	100	x	x
$PTSAxH_2O$	0,1	oDCB	100	✓	✓
AcOH		-	100	✓	✓
TFA		-	80	x	
$ZrCl_4$	0,05	oDCB	100	✓	✓
BBr_3	2	oDCB	100	✓	✓
$PTSAxH_2O$/prop. acid	3.5	oDCB	100	✓	✓
$TiCl_4$	6.2	oDCB	100	✓	x
$SnCl_4$/$PTSAxH_2O$	0.5/1	Pentanol	100	✓	x
H_2SO_4	3,7	oDCB	100	✓	✓
PPTS	0,1	oDCB	100	✓	✓
CSA	0,1	oDCB	100	✓	✓
$SbCl_5$	6	oDCB	100	✓	✓
$FeCl_3$	0,1	oDCB	100	✓	✓
$HCl_{(g)}$		Dioxan	80	x	x
$HCl_{(g)}$		DMSO	80	x	x
Conc. HCl		-	100	✓	✓
$PTSAxH_2O$	0,1	DMSO	100	x	x
BF_3	0,1	DMSO	100	✓	✓
$SiCl_4$	0,1	oDCB	100	✓	✓
$NbCl_5$	0,1	oDCB	100	✓	✓
VCl_3	0,1	oDCB	100	✓	✓
MSA	0,1	oDCB	100	✓	✓
CSA[3]	0,1	oDCB	80/100	✓	✓
$PTSAxH_2O$[3]	0,1	oDCB	80/100	✓	✓

[3] Reactions were kept at 80 ˚C for 10 days. After that time the reaction temperature was increased to 100˚C for an additional 5 days.

6 Bibliography

1. Karthik, P. S., Himaja, A. L. & Singh, S. P. Carbon-allotropes: synthesis methods, applications and future perspectives. *Carbon Lett.* **15**, 219–237 (2014).
2. Falcao, E. H. & Wudl, F. Carbon allotropes: beyond graphite and diamond. *J. Chem. Technol. Biotechnol.* **82**, 524–531 (2007).
3. Kroto, H. W., Heath, J. R., O'Brien, S. C., Curl, R. F. & Smalley, R. E. C60: Buckminsterfullerene. *Nature* **318**, 162–163 (1985).
4. Diederich, F. & Kivala, M. All-Carbon Scaffolds by Rational Design. *Adv. Mater.* **22**, 803–812 (2010).
5. Diederich, F. & Rubin, Y. Synthetic Approaches toward Molecular and Polymeric Carbon Allotropes. *Angew. Chem. Int. Ed. Engl.* **31**, 1101–1123 (1992).
6. O'Keeffe, M., Adams, G. B. & Sankey, O. F. Predicted new low energy forms of carbon. *Phys. Rev. Lett.* **68**, 2325–2328 (1992).
7. Hirsch, A. The era of carbon allotropes. *Nat. Mater.* **9**, 868–871 (2010).
8. Fan, Q. *et al.* Biphenylene network: A nonbenzenoid carbon allotrope. *Science* **372**, 852–856 (2021).
9. Iijima, S. Helical microtubules of graphitic carbon. *Nature* **354**, 56–58 (1991).
10. Novoselov, K. S. *et al.* Electric Field Effect in Atomically Thin Carbon Films. *Science* **306**, 666–669 (2004).
11. Hu, Y. *et al.* Synthesis of γ-graphyne using dynamic covalent chemistry. *Nat. Synth.* (2022) doi:10.1038/s44160-022-00068-7.
12. Karfunkel, H. R. & Dressler, T. New hypothetical carbon allotropes of remarkable stability estimated by MNDO solid-state SCF computations. *J. Am. Chem. Soc.* **114**, 2285–2288 (1992).
13. Krätschmer, W., Lamb, L. D., Fostiropoulos, K. & Huffman, D. R. Solid C60: a new form of carbon. *Nature* **347**, 354–358 (1990).
14. Tohji, K. *et al.* Selective and High-Yield Synthesis of Higher Fullerenes. *J. Phys. Chem.* **99**, 17785–17788 (1995).
15. Georgakilas, V., Perman, J. A., Tucek, J. & Zboril, R. Broad Family of Carbon Nanoallotropes: Classification, Chemistry, and Applications of Fullerenes, Carbon Dots, Nanotubes, Graphene, Nanodiamonds, and Combined Superstructures. *Chem. Rev.* **115**, 4744–4822 (2015).
16. Umeyama, T. & Imahori, H. Electron transfer and exciplex chemistry of functionalized nanocarbons: effects of electronic coupling and donor dimerization. *Nanoscale Horiz.* **3**, 352–366 (2018).
17. Imahori, H. Creation of Fullerene-Based Artificial Photosynthetic Systems. *Bull. Chem. Soc. Jpn.* **80**, 621–636 (2007).

18. Guldi, D. M., Illescas, B. M., Atienza, C. M., Wielopolski, M. & Martín, N. Fullerene for organic electronics. *Chem. Soc. Rev.* **38**, 1587 (2009).
19. Collavini, S. & Delgado, J. L. Fullerenes: the stars of photovoltaics. *Sustain. Energy Fuels* **2**, 2480–2493 (2018).
20. Hirsch, A. & Brettreich, M. *Fullerenes: Chemistry and Reactions*. (Wiley, 2004). doi:10.1002/3527603492.
21. Monthioux, M. & Kuznetsov, V. L. Who should be given the credit for the discovery of carbon nanotubes? *Carbon* **44**, 1621–1623 (2006).
22. L.V. Radushkevich & V.M. Lukianovich. About carbon structure, formed by thermal decomposition of carbon monoxide at iron contact. *Zhurn Fiz Khim* **XXVI**, 88–95 (1952).
23. Iijima, S. & Ichihashi, T. Single-shell carbon nanotubes of 1-nm diameter. *Nature* **363**, 603–605 (1993).
24. Thomsen, C., Reich, S. & Maultzsch, J. *Carbon Nanotubes: Basic Concepts and Physical Properties*. (Wiley, 2004). doi:10.1002/9783527618040.
25. Norizan, M. N. *et al.* Carbon nanotubes: functionalisation and their application in chemical sensors. *RSC Adv.* **10**, 43704–43732 (2020).
26. Hassan, A. G. *et al.* Effects of varying electrodeposition voltages on surface morphology and corrosion behavior of multi-walled carbon nanotube coated on porous Ti-30 at.%-Ta shape memory alloys. *Surf. Coat. Technol.* **401**, 126257 (2020).
27. Souto, L. F. C. & Soares, B. G. Polyaniline/carbon nanotube hybrids modified with ionic liquids as anticorrosive additive in epoxy coatings. *Prog. Org. Coat.* **143**, 105598 (2020).
28. Medupin, R. O., Abubakre, O. K., Abdulkareem, A. S., Muriana, R. A. & Abdulrahman, A. S. Carbon Nanotube Reinforced Natural Rubber Nanocomposite for Anthropomorphic Prosthetic Foot Purpose. *Sci. Rep.* **9**, 20146 (2019).
29. Zhou, E. *et al.* Synergistic effect of graphene and carbon nanotube for high-performance electromagnetic interference shielding films. *Carbon* **133**, 316–322 (2018).
30. Feng, D., Xu, D., Wang, Q. & Liu, P. Highly stretchable electromagnetic interference (EMI) shielding segregated polyurethane/carbon nanotube composites fabricated by microwave selective sintering. *J. Mater. Chem. C* **7**, 7938–7946 (2019).
31. Guo, F. *et al.* Advanced Lithium Metal–Carbon Nanotube Composite Anode for High-Performance Lithium–Oxygen Batteries. *Nano Lett.* **19**, 6377–6384 (2019).
32. Cataldo, S., Salice, P., Menna, E. & Pignataro, B. Carbon nanotubes and organic solar cells. *Energy Env. Sci* **5**, 5919–5940 (2012).
33. Liu, C. *et al.* Hydrogen Storage in Single-Walled Carbon Nanotubes at Room Temperature. *Science* **286**, 1127–1129 (1999).
34. Rinzler, A. G. *et al.* Unraveling Nanotubes: Field Emission from an Atomic Wire. *Science* **269**, 1550–1553 (1995).

35. Geim, A. K. & Novoselov, K. S. The rise of graphene. in *Nanoscience and Technology* 11–19 (Co-Published with Macmillan Publishers Ltd, UK, 2009). doi:10.1142/9789814287005_0002.
36. Wallace, P. R. The Band Theory of Graphite. *Phys. Rev.* **71**, 622–634 (1947).
37. Pulizzi, F. *et al.* Graphene in the making. *Nat. Nanotechnol.* **14**, 914–918 (2019).
38. Morozov, S. V. *et al.* Giant Intrinsic Carrier Mobilities in Graphene and Its Bilayer. *Phys. Rev. Lett.* **100**, 016602 (2008).
39. Lee, C., Wei, X., Kysar, J. W. & Hone, J. Measurement of the Elastic Properties and Intrinsic Strength of Monolayer Graphene. *Science* **321**, 385–388 (2008).
40. Balandin, A. A. Thermal properties of graphene and nanostructured carbon materials. *Nat. Mater.* **10**, 569–581 (2011).
41. Nair, R. R. *et al.* Fine Structure Constant Defines Visual Transparency of Graphene. *Science* **320**, 1308–1308 (2008).
42. Moser, J., Barreiro, A. & Bachtold, A. Current-induced cleaning of graphene. *Appl. Phys. Lett.* **91**, 163513 (2007).
43. Liu, J., Tang, J. & Gooding, J. J. Strategies for chemical modification of graphene and applications of chemically modified graphene. *J. Mater. Chem.* **22**, 12435 (2012).
44. Bonaccorso, F., Sun, Z., Hasan, T. & Ferrari, A. C. Graphene photonics and optoelectronics. *Nat. Photonics* **4**, 611–622 (2010).
45. Rahimi, S. *et al.* Toward 300 mm Wafer-Scalable High-Performance Polycrystalline Chemical Vapor Deposited Graphene Transistors. *ACS Nano* **8**, 10471–10479 (2014).
46. Noh, Y.-J. *et al.* High-performance polymer solar cells with radiation-induced and reduction-controllable reduced graphene oxide as an advanced hole transporting materi*al. Carbon* **79**, 321–329 (2014).
47. Huang, H. *et al.* The Chemistry and Promising Applications of Graphene and Porous Graphene Materials. *Adv. Funct. Mater.* **30**, 1909035 (2020).
48. Chung, D. D. L. Review Graphite. *J. Mater. Sci.* **37**, 1475–1489 (2002).
49. Janiak, C., Meyer, H.-J., Gudat, D. & Kurz, P. *Riedel Moderne Anorganische Chemie*. (De Gruyter, 2018). doi:10.1515/9783110441635.
50. Williams, O. A. Nanocrystalline diamond. *Diam. Relat. Mater.* **20**, 621–640 (2011).
51. Smalley, R. E. Discovering the Fullerenes(Nobel Lecture). *Angew. Chem. Int. Ed. Engl.* **36**, 1594–1601 (1997).
52. Geim, A. K. Nobel Lecture: Random walk to graphene. *Rev. Mod. Phys.* **83**, 851–862 (2011).
53. Adams, G. B., O'Keeffe, M., Sankey, O. F. & Page, J. B. Polybenzene, A Predicted New Low Energy Form of Carbon. *MRS Proc.* **270**, 103 (1992).
54. *CRC handbook of chemistry and physics: a ready-reference book of chemical and physical data*. (CRC Press, 2019).
55. Yaghi, O. M. Reticular Chemistry in All Dimensions. *ACS Cent. Sci.* **5**, 1295–1300 (2019).

56. Ockwig, N. W., Delgado-Friedrichs, O., O'Keeffe, M. & Yaghi, O. M. Reticular Chemistry: Occurrence and Taxonomy of Nets and Grammar for the Design of Frameworks. *Acc. Chem. Res.* **38**, 176–182 (2005).
57. Diercks, C. S. & Yaghi, O. M. The atom, the molecule, and the covalent organic framework. *Science* **355**, eaal1585 (2017).
58. Jiang, H., Alezi, D. & Eddaoudi, M. A reticular chemistry guide for the design of periodic solids. *Nat. Rev. Mater.* **6**, 466–487 (2021).
59. Haase, F. & Lotsch, B. V. Solving the COF trilemma: towards crystalline, stable and functional covalent organic frameworks. *Chem. Soc. Rev.* **49**, 8469–8500 (2020).
60. Côté, A. P. *et al.* Porous, Crystalline, Covalent Organic Frameworks. *Science* **310**, 1166–1170 (2005).
61. Uribe-Romo, F. J. *et al.* A Crystalline Imine-Linked 3-D Porous Covalent Organic Framework. *J. Am. Chem. Soc.* **131**, 4570–4571 (2009).
62. Bourda, L., Krishnaraj, C., Van Der Voort, P. & Van Hecke, K. Conquering the crystallinity conundrum: efforts to increase quality of covalent organic frameworks. *Mater. Adv.* **2**, 2811–2845 (2021).
63. Smith, B. J. & Dichtel, W. R. Mechanistic Studies of Two-Dimensional Covalent Organic Frameworks Rapidly Polymerized from Initially Homogenous Conditions. *J. Am. Chem. Soc.* **136**, 8783–8789 (2014).
64. Smith, B. J., Overholts, A. C., Hwang, N. & Dichtel, W. R. Insight into the crystallization of amorphous imine-linked polymer networks to 2D covalent organic frameworks. *Chem. Commun.* **52**, 3690–3693 (2016).
65. Haase, F. *et al.* Topochemical conversion of an imine- into a thiazole-linked covalent organic framework enabling real structure analysis. *Nat. Commun.* **9**, 2600 (2018).
66. Stewart, D. *et al.* Stable and ordered amide frameworks synthesised under reversible conditions which facilitate error checking. *Nat. Commun.* **8**, 1102 (2017).
67. Karak, S. *et al.* Constructing Ultraporous Covalent Organic Frameworks in Seconds via an Organic Terracotta Process. *J. Am. Chem. Soc.* **139**, 1856–1862 (2017).
68. Karak, S., Kumar, S., Pachfule, P. & Banerjee, R. Porosity Prediction through Hydrogen Bonding in Covalent Organic Frameworks. *J. Am. Chem. Soc.* **140**, 5138–5145 (2018).
69. Matsumoto, M. *et al.* Rapid, Low Temperature Formation of Imine-Linked Covalent Organic Frameworks Catalyzed by Metal Triflates. *J. Am. Chem. Soc.* **139**, 4999–5002 (2017).
70. Spitler, E. L., Giovino, M. R., White, S. L. & Dichtel, W. R. A mechanistic study of Lewis acid-catalyzed covalent organic framework formation. *Chem Sci* **2**, 1588–1593 (2011).
71. Calik, M. *et al.* From Highly Crystalline to Outer Surface-Functionalized Covalent Organic Frameworks—A Modulation Approach. *J. Am. Chem. Soc.* **138**, 1234–1239 (2016).
72. Ma, T. *et al.* Single-crystal x-ray diffraction structures of covalent organic frameworks. *Science* **361**, 48–52 (2018).

73. Zhang, W. *et al.* Reconstructed covalent organic frameworks. *Nature* **604**, 72–79 (2022).
74. Zhao, D. *et al.* Triblock Copolymer Syntheses of Mesoporous Silica with Periodic 50 to 300 Angstrom Pores. *Science* **279**, 548–552 (1998).
75. Kresge, C. T., Leonowicz, M. E., Roth, W. J., Vartuli, J. C. & Beck, J. S. Ordered mesoporous molecular sieves synthesized by a liquid-crystal template mechanism. *Nature* **359**, 710–712 (1992).
76. Stupp, S. I., Son, S., Lin, H. C. & Li, L. S. Synthesis of Two-Dimensional Polymers. *Science* **259**, 59–63 (1993).
77. Mazur, M. *et al.* Synthesis of 'unfeasible' zeolites. *Nat. Chem.* **8**, 58–62 (2016).
78. Roth, W. J. *et al.* A family of zeolites with controlled pore size prepared using a top-down method. *Nat. Chem.* **5**, 628–633 (2013).
79. Liu, W. *et al.* Two-Dimensional Polymer Synthesized *via* Solid-State Polymerization for High-Performance Supercapacitors. *ACS Nano* **12**, 852–860 (2018).
80. Liu, W. *et al.* A two-dimensional conjugated aromatic polymer via C–C coupling reaction. *Nat. Chem.* **9**, 563–570 (2017).
81. Tahir, N., Krishnaraj, C., Leus, K. & Van Der Voort, P. Development of Covalent Triazine Frameworks as Heterogeneous Catalytic Supports. *Polymers* **11**, 1326 (2019).
82. Kuhn, P., Antonietti, M. & Thomas, A. Porous, Covalent Triazine-Based Frameworks Prepared by Ionothermal Synthesis. *Angew. Chem. Int. Ed.* **47**, 3450–3453 (2008).
83. Katekomol, P., Roeser, J., Bojdys, M., Weber, J. & Thomas, A. Covalent Triazine Frameworks Prepared from 1,3,5-Tricyanobenzene. *Chem. Mater.* **25**, 1542–1548 (2013).
84. Bojdys, M. J., Jeromenok, J., Thomas, A. & Antonietti, M. Rational Extension of the Family of Layered, Covalent, Triazine-Based Frameworks with Regular Porosity. *Adv. Mater.* **22**, 2202–2205 (2010).
85. Liu, X. *et al.* Enhanced carbon dioxide uptake by metalloporphyrin-based microporous covalent triazine framework. *Polym. Chem.* **4**, 2445 (2013).
86. Bhunia, A., Boldog, I., Möller, A. & Janiak, C. Highly stable nanoporous covalent triazine-based frameworks with an adamantane core for carbon dioxide sorption and separation. *J. Mater. Chem. A* **1**, 14990 (2013).
87. Bhunia, A., Vasylyeva, V. & Janiak, C. From a supramolecular tetranitrile to a porous covalent triazine-based framework with high gas uptake capacities. *Chem. Commun.* **49**, 3961 (2013).
88. Meyer, E. A., Castellano, R. K. & Diederich, F. Interactions with Aromatic Rings in Chemical and Biological Recognition. *Angew. Chem. Int. Ed.* **42**, 1210–1250 (2003).
89. Dougherty, D. A. Cation-π Interactions in Chemistry and Biology: A New View of Benzene, Phe, Tyr, and Trp. *Science* **271**, 163–168 (1996).
90. Elmorsy, S. S., Pelter, A. & Smith, K. The direct production of tri- and hexa-substituted benzenes from ketones under mild conditions. *Tetrahedron Lett.* **32**, 4175–4176 (1991).

91. Wagh, G. D. & Akamanchi, K. G. Sulfated tungstate catalyzed synthesis of C 3 -symmetric 1,3,5-triaryl benzenes under solvent-free condition. *Tetrahedron Lett.* **58**, 3032–3036 (2017).
92. Safaei, H. R., Davoodi, M. & Shekouhy, M. Highly Efficient Synthesis of Substituted Benzenes in the Presence of $B(HSO_4)_3$ as a New and Reusable Catalyst Under Solvent-Free Conditions. *Synth. Commun.* **43**, 2178–2190 (2013).
93. Frantz, D. K., Walish, J. J. & Swager, T. M. Synthesis and Properties of the 5,10,15-Trimesityltruxen-5-yl Radic*al. Org. Lett.* **15**, 4782–4785 (2013).
94. Li, Z., Sun, W.-H., Jin, X. & Shao, C. Triple Self-Condensation of Ketones Yielding Aromatics Promoted with Titanium Tetrachloride. *Synlett* **2001**, 1947–1949 (2001).
95. Boorum, M. M., Vasil'ev, Y. V., Drewello, T. & Scott, L. T. Groundwork for a Rational Synthesis of C_{60} : Cyclodehydrogenation of a $C_{60}H_{30}$ Polyarene. *Science* **294**, 828–831 (2001).
96. Sanchez-Valencia, J. R. *et al.* Controlled synthesis of single-chirality carbon nanotubes. *Nature* **512**, 61–64 (2014).
97. Dehmlow, E. V. & Kelle, T. Synthesis of New Truxene Derivatives: Possible Precursors of Fullerene Partial Structures? *Synth. Commun.* **27**, 2021–2031 (1997).
98. Boorum, M. M. & Scott, L. T. The Synthesis of Tris-Annulated Benzenes by Aldol Trimerization of Cyclic Ketones. in *Modern Arene Chemistry* (ed. Astruc, D.) 20–31 (Wiley-VCH Verlag GmbH & Co. KGaA, 2002). doi:10.1002/3527601767.ch1.
99. Amick, A. W. & Scott, L. T. Trisannulated Benzene Derivatives by Acid Catalyzed Aldol Cyclotrimerizations of Cyclic Ketones. Methodology Development and Mechanistic Insight. *J. Org. Chem.* **72**, 3412–3418 (2007).
100. Sedenkova, K. N. *et al.* Beyond the Dimer and Trimer: Tetraspiro[2.1.2 ^{5} .1.2 ^{9} .1.2 ^{13} .1 ^{3}] hexadecane-1,3,5,7-tetraone—the Cyclic Tetramer of Carbonylcyclopropane. *Chem. – Eur. J.* **22**, 3996–3999 (2016).
101. Braams, J. F. H., Bos, H. J. T. & Arens, J. F. Chemistry of acetylenic ethers. Part 90: Cyclotetramerization of ethynyl ethers to 1,3,5,7-tetra-alkoxycyclo-octatetraenes. Syntheses of 3,5,7-triethoxy-2,4,6-cyclo-octatrienone and of 1,3,5,7-tetra-alkoxy-2,6-dioxa-adamantanes. *Recl. Trav. Chim. Pays-Bas* **87**, 193–200 (2010).
102. Samoshin, V. V., Gremyachinskiy, D. E., Smith, L. L., Bliznets, I. V. & Gross, P. H. Practical synthesis of bis-homoallylic alcohols from dialdehydes or their acetals. *Tetrahedron Lett.* **43**, 6329–6330 (2002).
103. Schelhaas, M. & Waldmann, H. Protecting Group Strategies in Organic Synthesis. *Angew. Chem. Int. Ed. Engl.* **35**, 2056–2083 (1996).
104. VanRheenen, V., Kelly, R. C. & Cha, D. Y. An improved catalytic OsO4 oxidation of olefins to -1,2-glycols using tertiary amine oxides as the oxidant. *Tetrahedron Lett.* **17**, 1973–1976 (1976).

105. Matsubara, S. *et al.* [2+1] Cycloaddition reaction of bis(iodozincio)methane with 1,2-diketones: face-to-face complex of bis(iodozincio)methane and 1,2-diketones as a reaction intermediate. *Tetrahedron* **58**, 8255–8262 (2002).
106. Ukai, K., Oshima, K. & Matsubara, S. Preparation of Cyclopropanediol: Novel [2 + 1] Cycloaddition Reaction of Bis(iodozincio)methane with 1,2-Diketones. *J. Am. Chem. Soc.* **122**, 12047–12048 (2000).
107. Weiss, U. & Edwards, J. M. A one-step synthesis of ketonic compounds of the pentalane, [3,3,3]- and [4,3,3]-propellane series. *Tetrahedron Lett.* **9**, 4885–4887 (1968).
108. Cadieux, J. A., Buller, D. J. & Wilson, P. D. Versatile Route to *centro* -Substituted Triquinacene Derivatives: Synthesis of 10-Phenyltriquinacene. *Org. Lett.* **5**, 3983–3986 (2003).
109. Liang, H. *et al.* Tailoring the Performance of Vegetable Oil-Based Waterborne Polyurethanes through Incorporation of Rigid Cyclic Rings into Soft Polymer Networks. *ACS Sustain. Chem. Eng.* **8**, 914–925 (2020).
110. Lannoye, G., Sambasivarao, K., Wehrli, S., Cook, J. M. & Weiss, U. General approach to the synthesis of polyquinenes via the Weiss reaction. 6. Progress toward the synthesis of dicyclopentapentalenes. *J. Org. Chem.* **53**, 2327–2340 (1988).
111. Huang, D., Zhao, Y. & Newhouse, T. R. Synthesis of Cyclic Enones by Allyl-Palladium-Catalyzed α,β-Dehydrogenation. *Org. Lett.* **20**, 684–687 (2018).
112. Chen, Y., Romaire, J. P. & Newhouse, T. R. Palladium-Catalyzed α,β-Dehydrogenation of Esters and Nitriles. *J. Am. Chem. Soc.* **137**, 5875–5878 (2015).
113. Ito, Y., Hirao, T. & Saegusa, T. Synthesis of .alpha.,.beta.-unsaturated carbonyl compounds by palladium(II)-catalyzed dehydrosilylation of silyl enol ethers. *J. Org. Chem.* **43**, 1011–1013 (1978).
114. Larock, R. C., Hightower, T. R., Kraus, G. A., Hahn, P. & Zheng, D. A simple, effective, new, palladium-catalyzed conversion of enol silanes to enones and enals. *Tetrahedron Lett.* **36**, 2423–2426 (1995).
115. Trost, B. M., Salzmann, T. N. & Hiroi, K. New synthetic reactions. Sulfenylations and dehydrosulfenylations of esters and ketones. *J. Am. Chem. Soc.* **98**, 4887–4902 (1976).
116. Nicolaou, K. C., Zhong, Y.-L. & Baran, P. S. A New Method for the One-Step Synthesis of α,β-Unsaturated Carbonyl Systems from Saturated Alcohols and Carbonyl Compounds. *J. Am. Chem. Soc.* **122**, 7596–7597 (2000).
117. Horii, K. *et al.* Bis-periazulene (Cyclohepta[*def*]fluorene) as a Nonalternant Isomer of Pyrene: Synthesis and Characterization of Its Triaryl Derivatives. *J. Am. Chem. Soc.* **144**, 3370–3375 (2022).
118. Bertz, S. H. The conversion of bicyclo[3.3.0]octane-3,7-dione to bicyclo[3.3.0]oct-1-ene-3,7-dione. Symmetry as a complicating factor in synthetic analysis. *Tetrahedron Lett.* **24**, 5577–5580 (1983).

119. Ogliaruso, M. A., Romanelli, M. G. & Becker, E. I. Chemistry of Cyclopentadienones. *Chem. Rev.* **65**, 261–367 (1965).
120. Docken, A. M. Bicyclo[3.3.0]octa-1,5-diene-3,7-dione. *J. Org. Chem.* **46**, 4096–4097 (1981).
121. Dermont Michael O'Hare & Ashley Andrew Edward. Pentalenes. (2008).
122. Yates, P., Hand, E. S. & French, G. B. Schroeter and Vossen's "Red Salt" and Related Bicyclo[3.3.0]octane Derivatives [1]. *J. Am. Chem. Soc.* **82**, 6347–6353 (1960).
123. Tsunoda, T., Suzuki, M. & Noyori, R. A facile procedure for acetalization under aprotic conditions. *Tetrahedron Lett.* **21**, 1357–1358 (1980).
124. Chandler, C. L. & List, B. Catalytic, Asymmetric Transannular Aldolizations: Total Synthesis of (+)-Hirsutene. *J. Am. Chem. Soc.* **130**, 6737–6739 (2008).
125. Minnaard, A. J., B.P.A. Wijnberg, J. & Groot, A. de. The synthesis of (+)-hedycaryol, starting from natural (−)-guaiol. *Tetrahedron* **50**, 4755–4764 (1994).
126. Piers, E., Skupinska, K. A. & Wallace, D. J. CuCN-Mediated Intramolecular Conjugate Additions. Syntheses of Functionalized, *cis* -Fused Bicyclo[6.3.0]undecanes, Bicyclo[6.4.0]dodecanes, and Bicyclo[7.4.0]tridecanes. *Synlett* **1999**, 1867–1870 (1999).
127. Dash, B. P., Satapathy, R., Maguire, J. A. & Hosmane, N. S. Synthesis of a New Class of Carborane-Containing Star-Shaped Molecules via Silicon Tetrachloride Promoted Cyclotrimerization Reactions. *Org. Lett.* **10**, 2247–2250 (2008).
128. Elmorsy, S. S., Pelter, A., Smith, K., Hursthouse, M. B. & Ando, D. Investigations of the tetrachlorosilane-ethanol induced self condensations of ketones. *Tetrahedron Lett.* **33**, 821–824 (1992).
129. Bock, H., Rajaoarivelo, M., Clavaguera, S. & Grelet, É. An Efficient Route to Stable Room-Temperature Liquid-Crystalline Triphenylenes. *Eur. J. Org. Chem.* **2006**, 2889–2893 (2006).
130. Jing, X. *et al.* Novel Method for the Synthesis of 1,3,5-Triarylbenzenes from Ketones. *Synth. Commun.* **35**, 3167–3171 (2005).
131. Zhao, Y. *et al.* PTSA-catalyzed green synthesis of 1,3,5-triarylbenzene under solvent-free conditions. *Green Chem.* **12**, 1370 (2010).
132. Sampey, J. R. sym-Tritolylbenzene. *J. Am. Chem. Soc.* **62**, 1953–1953 (1940).
133. Lyle, R. E., DeWitt, E. J., Nichols, N. M. & Cleland, W. Acid Catalyzed Condensations. I. 1,3,5-Triarylbenzenes [1]. *J. Am. Chem. Soc.* **75**, 5959–5961 (1953).
134. Baalouch, M., De Mesmaeker, A. & Beaudegnies, R. Efficient synthesis of bicyclo[3.2.1]octane-2,4-diones and their incorporation into potent HPPD inhibitors. *Tetrahedron Lett.* **54**, 557–561 (2013).
135. Feng, C.-G., Wang, Z.-Q., Shao, C., Xu, M.-H. & Lin, G.-Q. Highly Practical Catalytic Asymmetric 1,4-Addition of Arylboronic Acids in Water Using New Hydrophilic Chiral Bicyclo[3.3.0] Diene Ligands. *Org. Lett.* **10**, 4101–4104 (2008).

136. Quindt, M. I., Gola, G. F., Ramirez, J. A. & Bonesi, S. M. Photo-Fries Rearrangement of Some 3-Acylestrones in Homogeneous Media: Preparative and Mechanistic Studies. *J. Org. Chem.* **84**, 7051–7065 (2019).
137. Suto, M. J., Tramposch, K. M., Wierzba, M., Solo, A. J. & Duax, W. Approaches to the synthesis of ring C transposed progesterone analogs: rac-7.beta.,15.alpha.-ethano-11,12-seco-11,19-bisnor-17.alpha.-pregn-4-ene-3,20-dione and rac-4,4-dimethyl-7,7-(ethylenedioxy)-4a.alpha.,4b.beta.,8a.alpha.,10a.beta.-perhydro-3-phenanthrenone. *J. Org. Chem.* **52**, 2263–2273 (1987).
138. Feng, X., Mu, H., Xiang, Z. & Cai, Y. Theoretical investigation of negatively curved 6.8 2 D carbon based on density functional theory. *Comput. Mater. Sci.* **171**, 109211 (2020).